Research Square

Preprints are preliminary reports that have not undergone peer review.
They should not be considered conclusive, used to inform clinical practice,
or referenced by the media as validated information.

Synoptic–Thermodynamic Controls of Thunderstorm Activity over Khanaqin: A 30-Year Analysis of Instability Indices and Jet Stream Dynamics

Imad Abdulridha Al-Khulaifawi

imadjasim900@gmail.com

Southern Federal University

Aqeel Ghazi Mutar[2]

Mustansiriyah University

Research Article

Keywords: Thunderstorm, Temperature, Dew point temperature, K-index, Totals-Totals Index, CAPE, Khanaqin

Posted Date: June 20th, 2026

DOI: https://doi.org/10.21203/rs.3.rs-9829160/v1

License: This work is licensed under a Creative Commons Attribution 4.0 International License.
Read Full License

Additional Declarations: No competing interests reported.

Version of Record: A version of this preprint was published at Theoretical and Applied Climatology on October 10th, 2026. See the published version at https://doi.org/10.1007/s00704-026-06594-0.

Synoptic–Thermodynamic Controls of Thunderstorm Activity over Khanaqin: A 30-Year Analysis of Instability Indices and Jet Stream Dynamics

Imad Abdulridha Jasim Al-Khulaifawi [1*]

Aqeel Ghazi Mutar[2]

[1]PhD student of the Department of Oceanology, Institute of Earth Sciences, Southern Federal University, Russia.

[2]Department of Atmospheric Sciences, College of Science, Mustansiriyah University, Iraq.

imadjasim900@gmail.com

https://orcid.org/0009-0008-1610-9795

Abstract: This work aims to analyze the climatic and physical characteristics of thunderstorms over the city of Khanaqin in eastern Iraq by integrating surface observational data with global reanalysis data from 1990 to 2019. Recordings from the Khanaqin meteorological station were used to identify thunderstorm days, along with ERA-5 and MERRA-2 data to analyze the thermal, humid, and dynamic properties of the atmosphere, particularly in the upper atmosphere associated with jet streams. Time-based statistical analysis of thunderstorm oscillations was performed, and indices of atmospheric instability (K-index, Total Totals index, and CAPE) were calculated. Their relationship to the vertical structure of thunderstorms was investigated, including the updraft level, equilibrium level, and cloud thickness. MERRA-2 data were also employed in synoptic analysis to characterize the role of jet streams and upper divergence in driving deep convection. The results showed that thunderstorm activity in the study area exhibited clear annual and seasonal oscillations without a statistically significant medium-term trend. The majority of storms occurred during the spring season, in an atmospheric environment characterized by moderate thermal instability, with CAPE values generally below 1000 J/kg. Despite these findings, deep thunderstorms with significant vertical extent were observed, indicating the crucial role of large-scale dynamic factors, particularly upper-level troughs and jet stream coupling, in enhancing storm intensity. The study reveals that thunderstorms in eastern Iraq are primarily regulated by upper-level synoptic influences rather than solely by convection energy, highlighting the limitations of using CAPE as a sole indicator for estimating storm intensity in semi-arid environments. These results contribute to a more profound understanding of convection mechanisms in areas with limited observational data and provide an important scientific basis for developing weather forecasting and severe storm early warning systems in Iraq and neighboring regions.

Keywords: Thunderstorm, Temperature, Dew point temperature, K-index, Totals-Totals Index, CAPE, Khanaqin.

1. Introduction

Thunderstorms are characterized by thermal clouds with a significant vertical extension. The peaks can usually reach the level of the tropopause, and their bases will be located near the highest boundary of the boundary layer (Wang, 2013). Thunderstorms are significant and potentially dangerous atmospheric phenomena. Some thunderstorms can produce little to no precipitation, but they can be associated with powerful winds, heavy rain, and occasionally snow, sleet, or hail. Known as a squall line, thunderstorms can form a rain band or line. Layers of warm, humid air rise to colder areas of the atmosphere in a massive, quick updraft to form thunderstorms. Updraft moisture condenses there to create cumulonimbus clouds, which in turn produce heavy rainfall, snow, large hail, powerful tornadoes, destructive winds, and windstorms (Brázdil et al., 2020; Kolendowicz et al., 2017; Krider, 2021; Pekárová

et al., 2021; Púčik et al., 2013; Roy et al., 2023; Taszarek et al., 2020). It is impossible to assume that the frequency of severe thunderstorms can remain constant, so there is serious worry and interest in studying how these storms may react to a warming and possibly more changeable environment. The Coupled Model Intercomparison Project version 5 currently projects (moderate to high) warming scenarios for the year 2100 (Taylor, 2012). According to the model's findings, the near-surface air's capacity to hold water would be improved by raising the average surface temperature by 4 to 6 degrees Celsius. Consequently, atmospheric humidity levels increase by 25%, provided sufficient moisture is present (Agard & Emanuel, 2017; Dai, 2006; Gettleman et al., 2002; Romps, 2016; Willett et al., 2010). Rising temperature and humidity near the surface contribute to greater vertical thermodynamic instability. This instability, measured by convective available potential energy (CAPE), can happen either because the air is unstable on its own or because the air is lifted to a height where it is less dense than the surrounding air. Increased humidity is particularly significant, as a substantial portion of this potential energy arises from the phase changes of water during the ascent and cooling of air (Emanuel, 1994).

Atmospheric instability, adequate moisture in the lower troposphere, and lifting mechanisms (such as convection, frontal lift, and convergence) are the three fundamental conditions for thunderstorm development (Doswell, 1987; Doswell et al., 1996; Nssl, 2020). The developing, mature, and dissipation stages are the three phases that all thunderstorms (single, multicellular, and supercell storms), regardless of kind, go through. A severe thunderstorm may be so powerful that the top of the cumulus cloud can penetrate deep into the stable stratosphere. The cumulus clouds will continue to grow and combine with other cells to form a cumulus congestus cloud that extends even higher into the atmosphere. The apex of the cloud may occasionally reach over 18 kilometers (60,000 feet) above the ground (Roy et al., 2023; Taszarek et al., 2020). Indices like the K-index, Lifted Index, and Convective Available Potential Energy (CAPE) are crucial for meteorologists to assess regional convective potential. They help pinpoint areas with an unstable atmosphere, which is a key condition for thunderstorm development (Humood & Abbas, 2017).

Numerous attempts have been made to study the vertical structure of clouds in thunderstorms, including one by Zhao et al (2025) Which investigated the relationship between the polarimetric structure of thermal polarimetric radar and lightning activity during the life cycle of isolated thunderstorm cells. Using data from 15 separate thunderstorm cells and a dual-polarized S-band observatory to monitor polarimetric variables, the researchers demonstrated that changes in the microphysical content of supercooled water exhibit a strong correlation with lightning activity over short timescales (e.g., 6 minutes). This correlation reflects the relationship between airflow dynamics and microphysical transformation processes within the cloud during its development. The intensity of polarimetric radar waves depends on the increasing updraft and ice-forming processes that directly contribute to the activation of electrical charges within the cloud, which in turn affects lightning activity. Sokol et al (2023) Studied the vertical structure of lightning-producing thunderclouds using five years of Doppler polarimetric vertical cloud profiler data. The research compared storms producing strong electrical activity with those occurring at different distances from the measurement sites. The results indicate that the vertical structure of reflectivity and radar is closely related to lightning activity, with higher reflectivity values in the middle and upper levels associated with an increased probability of charge separation within the cloud and the role of large particles in the mixed-phase region in promoting the phenomenon. Peterson et al (2020) Investigated the classification of thunderstorm organization and structure using data from GOES Geostationary Lightning Mapper sensors. Their research highlights the importance of distinguishing between vertically convective regions, which produce heavy rainfall and lightning, and horizontally extending, less active stratiform regions. Space-based algorithms demonstrate how to identify the vertical structures of thunderstorms based on their microphysical components and lightning activity. This helps with better storm risk assessment and operational forecasting. The findings support a more profound understanding of how deep cloud structure relates to associated features such as rainfall intensity and lightning and demonstrate the value of integrating microphysical observations with electrical charge observations. Kolay et al (2025) This study analyzes thunderstorm activity at Istanbul International Airport using atmospheric stability indices data for the ground and upper levels that were obtained from the Turkish State Meteorological Service for 29 October 2018 and 1 January 2023. Thunderstorms were

seen to occur more frequently throughout the summer, with a total of 51 occurrences. With 32 thunderstorm events, June had the most of any month. This results in eight incidents annually (on average). Transitions between troughs and cold fronts accounted for 72.22% of the total. Compared to other stability indices, the K index and Total Totals index provided a better representation of the thunderstorm events. These two stability indicators accounted for 75% of the total thunderstorm days. During thunderstorms, convective available potential energy (CAPE) values are minimal, and the K and Total Totals indices are accurately reflected. This work contributes to a deeper scientific understanding of thunderstorm formation mechanisms in eastern Iraq (Khanaqin) by highlighting the complementary role of thermodynamic and large-scale dynamic factors and provides an important scientific basis for developing severe storm forecasting models in semi-arid regions under the influence of climate change. This study is limited by the absence of local upper-air sounding and weather radar data. However, the combined use of surface observations and high-resolution reanalysis datasets provides a robust framework for diagnosing thunderstorm dynamics in data-sparse regions. This study offers a thorough, medium-term investigation of Khanaqin's thermodynamic stability indices over a thirty-year period (1990–2019). This study seeks to address the disparity by conducting a statistical analysis of the temporal patterns of these indicators in semi-arid regions, specifically by assessing the characteristics of thunderstorms at Khanaqin Station during an average duration from 1990 to 2019. And the use of statistical techniques and humidity-based indicators such as TT and K provides an effective forecasting model for similar semi-arid regions around the world.

2. Materials and Methods

2.1. Study Area

Iraq is situated between 29°5′ and 37°22′N latitude and 38°45′–48°45′E longitude. Its geographical diversity includes mountainous regions in the north and northeast, plateau regions at lower altitudes to the south of the mountains, alluvial plains, and western plateaus. The elevation and location of these regions significantly influence the climatic conditions across Iraq. As one moves from south to north, temperatures decrease while rainfall increases (Al-Ansari, 2013; Sultan, 1986). Figure 1 shows the topography of Iraq and the location of the selected Khanaqin station. The city of Khanaqin is located in the northeastern part of Diyala Governorate in Iraq, near the Iranian border (approximately 8 km). It is the center of Khanaqin District and enjoys a strategic location on a major road connecting Iraq and Iran, adjacent to the Alwand River valley, which contributes to local agricultural activity. Khanaqin lies approximately at latitude 34.33° N and 45.38° E, at an elevation of approximately 180–185 meters above sea level, making it part of the relatively moderately elevated plains of eastern Iraq. The climate in Khanaqin is classified as a hot semi-arid climate, characterized by scorching, dry summers with maximum temperatures that can reach approximately 44°C, while winters are cooler with moderate rainfall compared to the other seasons. Rainfall is generally highest in late autumn and winter, with little or no rain during the summer months (Ibrahim and Al-Dabbas, 2021).

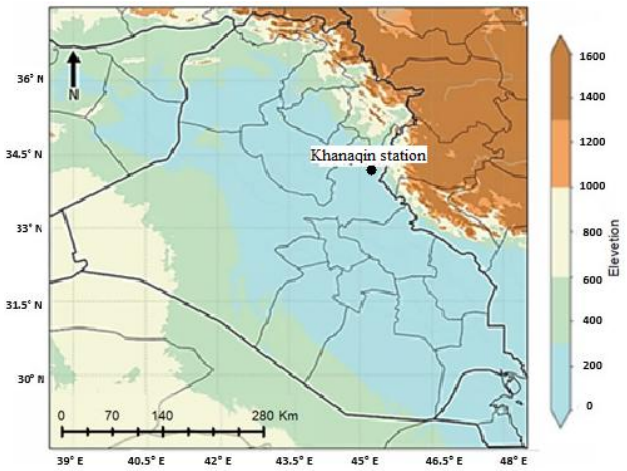


Figure 1. Elevation map of Iraq with the Khanaqin station highlighted

2.2. Data Set

The data used in this work included multiple sources such as the Iraqi General Authority for Meteorology and Seismic Monitoring (GAMSM), which provided data on thunderstorm weather conditions, surface temperature (T), dew point (Td), and sea level pressure (PPP) for the period (1990–2019). On the other hand, since the station lacked soundings (upper layer scanning) and radar data, reanalysis datasets (ERA5, MERRA-2) were used and validated before being used in the analysis of thunderstorm days. The reanalysis data from ERA5 for the period (1990-2019) are used with a temporal resolution of 00:00, 06:00, 12:00, and 18:00 UTC and a spatial resolution of 0.25° × 0.25° for the synoptic maps and parameters 850, 700, 500, and 300 hPa (Hersbach et al., 2023). The result was plotted using Origin Pro-21. The ERA5 is summarized in Table 1. In addition to ERA5, MERRA-2 (Modern-Era Retrospective Analysis for Research and Applications, Version 2) data from NASA, through its Global Modeling and Assimilation Office (GMAO), were also used. This study focuses on a point-scale analysis of a station that represents the interaction area between the mountain and the plain.

MERRA-2 data were primarily employed in upper-level synoptic analysis, specifically for wind speed distribution, streamlines, polar and subtropical jet stream analysis, and upper-level divergence at 300 hPa. MERRA-2 data is distinguished by its high capacity for representing large-scale dynamic fields, particularly in regions with few upper-level observation stations, such as the Middle East. It has been used to map wind speed and dynamic structure in the upper atmosphere, providing a more accurate characterization of the role of the jet stream and lower-level synoptic conditions in triggering thunderstorms. The MERRA-2 is summarized in Table 2.

While ERA-5 and MERRA-2 differ in spatial and temporal resolution, both datasets consistently depict the presence of upper-level jet structures during major thunderstorm events. Minor discrepancies in wind speed magnitude do not affect the synoptic interpretation.

Table 1: Overview of the ERA-5.

Characteristics	ERA5
Horizontal coverage	Global
Vertical coverage	1000 hPa to 1 hPa
Outputs	each 6h for upper-air
Horizontal resolution	Reanalysis: 0.25° × 0.25°
Vertical resolution	37 pressure levels
Data assimilation	Yes

Table 2: Overview of the MERRA-2.

Attribute	Description
Data type	Modern-Era Retrospective Analysis
Horizontal coverage	Global
Vertical coverage	Surface to 0.01 hPa
Primary pressure level used	300 hPa
Horizontal resolution	0.5° × 0.625°
Temporal resolution	3-hourly
Main application in this study	Jet stream analysis, wind speed, streamlines, weather diagnosis
Data provider	NASA - Global Modeling and Assimilation Office (GMAO)

3. Theoretical and Dynamical Framework

3.1. Diagnosis of Synoptic Conditions

Diagnosing the atmospheric conditions associated with a thunderstorm event can provide a clear picture of the dynamic causes and the general atmospheric flow pattern underlying the signal or trigger that initiated the baroclinic instability, which ultimately caused the event. Analyzing upper-level synoptic weather maps, spatial wind speed, and streamlines at the 300 hPa pressure level can reveal the nature of the polar jet stream's movement and its northward or southward meander patterns. This allows for the identification of the weather event's initiation and the intensity of the baroclinic instability, depending on the direction and amplitude of the meander pattern in the polar jet stream (Rossby wave). Identifying extratropical troughs and ridges at the 500 hPa pressure level is crucial for understanding how the Rossby wave's meander pattern deepens to form a mid-latitude depression, what the prevailing pattern is, and determining cyclogenesis. Meanwhile, the associated surface frontal system can be identified by analyzing surface wind patterns and surface temperature distributions (Mutar et al., 2021).

3.2. Calculations of Some Indices

3.2.1. K – Index

The amount and vertical extension of low-level moisture in the atmosphere, along with the vertical temperature lapse rate, are the foundations of the K-index, a thunderstorm potential indicator. The atmospheric conditions are indicated by K-index values in Table 3. The dew point temperature (Td at 850 mb) and the dew point depression for 700 mb (DD = T – Td), along with the temperatures at 850 mb and 500 mb (T), established the index value (Buck, 1981; George, 1960).

3.2.2. Total Totals Index

This analysis uses data on temperature and dew point at the 500 and 850 hPa levels. Cross totals (CT) and vertical totals (VT) comprise the Total Totals index. CT stands for the temperature differential and dew point between 850 and 500 hPa. In contrast, the temperature differential between 850 and 500 hPa is denoted as VT. The TTI is a tool for identifying potentially dangerous meteorological conditions. Information about the state of the atmosphere according to the value of the Total Totals index ranges of this parameter, as shown in Table 3 (Miller, 1972; U.S., 1990; Ye et al., 1998).

3.2.3. Convective Available Potential Energy (CAPE)

The integration of the vertical profile of the atmosphere was its basis. The atmosphere is stable when this parameter has smaller values. However, higher numbers indicate an unstable atmosphere (Lucas et al., 1994; Miller,

1972; Showalter, 1953). Table 3 displays information on the atmosphere's condition based on the value (CAPE) ranges of this parameter. In this formula:

LFC: is the free convection level, expressed in hPa or mb;

LE: level of equilibrium, expressed in hPa or mb;

Te: the surrounding temperature in degrees Celsius;

Tp: the temperature of the cloud parcel in degrees Celsius.

g: is the gravitational acceleration, expressed in m/s².

DZ is the layer's thickness between the LFC and EL levels, expressed in m or km.

Table 3: Atmospheric stability is based on the CAPE value (NWS, 2022; Ye et al., 1998).

Indices/ Parameter	Formula	Value (Indices/Parameter)	Thunderstorm Probability (Types)
K-Index	$K = T\ (850mb) + Td\ (850mb) - T\ (500mb) - DD\ (700mb)$	K below 20	Thunderstorms are unlikely or nonexistent
		K between 20 to 25	Isolated thunderstorms
		K between 26 to 30	Widely scattered thunderstorms with rain or severe weather
		K between 31 to 35	Scattered thunderstorms with heavy rain
		K above 35	Numerous thunderstorms with very heavy rain and hail
Total Totals Index	$TT = T850mb + Td850mb - 2(T500mb)$	TT below 45	Thunderstorm unlikely
		TT between 45 to 50	Thunderstorms possible
		TT between 51 to 52	Isolated severe thunderstorms
		TT between 53 to 56	Scattered severe thunderstorms
		TT above 56	Severe thunderstorms most likely, tornado
Convective Available Potential Energy (CAPE)	$CAPE = g * \int_{LFC}^{EL}(Tp - Te) * dz/Te$	CAPE below 300	Stable atmosphere
		CAPE 300 to 999	Marginally unstable atmosphere (light to moderate rain)
		CAPE 1000 to 2499	Moderately unstable atmosphere (heavy rain with small hail)
		CAPE 2500 to 3500	Very unstable atmosphere (very heavy rain with large hailstones)
		CAPE >3500	Extremely unstable atmosphere (tornado)

3.3. Lifting Condensation Level (LCL)

Using the LCL values, the cloud base height is roughly estimated, which is obtained using surface temperature and dew point temperature information (the air temperature equals the dew point temperature at this altitude). In order to calculate convective available potential energy (CAPE) and convective inhibition (CIN) and analyze thunderstorm potential and severity across any region, the LCL values are crucial. To determine the direct relationship with the total water vapor content, cloud height variability, seasonal and regional variability, etc., the LCL values can be employed as CBH (Craven et al., 2002; Xu et al., 2019**)**.

3.4. Equilibrium Level (EL)

The equilibrium level, or EL (Cinaroglu and Unutulmaz, 2018), is the height at which the temperature of the flowing air parcel equals the ambient temperature.

3.5. Cloud Thickness

The vertical thickness, measured in meters, refers to the depth or extent of the cloud. The disparity between the cloud's base and summit heights is known as this parameter. Due to the difficulty of precisely defining the cloud boundaries, the accuracy of determining this parameter ranges from 100 to 200 meters. The likelihood of dangerous meteorological phenomena of convective origin occurring increases with this value. Furthermore, an increase in cloud thickness signifies a rise in the phenomenon's intensity (Shmeter, 1972**)**.

4. Statistical Analysis

The K and Total Totals indices were selected due to their documented suitability for diagnosing convective potential in moisture-limited and semi-arid environments, where extreme CAPE values are uncommon. CAPE was used primarily to assess cloud vertical extent rather than storm frequency.

4.1. Monthly and Annual Frequency of Thunderstorms

Figure 2 shows the time distribution of the annual frequency of thunderstorms at Khanaqin station for the period from 1990 to 2019. The figure indicates that the number of thunderstorms has fluctuated significantly from year to year without showing a clear long-term trend towards increasing or decreasing. This fluctuation reflects the changing nature of the weather factors influencing the formation of thunderstorms, which are directly related to the dynamic and thermal conditions of the atmosphere in the region. The highest frequency of thunderstorms was recorded in 2008, with around 30 storms. In contrast, the lowest frequency was observed in 1990, with the number of storms not exceeding approximately three; this large difference between the lowest and highest frequency of thunderstorms over different years is due to the high variability that characterizes rainfall in Iraq in general (AL-Lami et al., 2024; Al-Muhyi et al., 2024). It is also noted that the periods of the mid-nineties (1993–1997) and the mid-first decade of the millennium (2006–2008) were characterized by a relative increase in the number of thunderstorms, which may coincide with periods active in terms of regional climate oscillations such as the North Atlantic Oscillation (NAO) or the El Niño-Southern Oscillation (ENSO), which affect rainfall patterns and atmospheric instability in the Middle East regions. An analysis of the number of Mediterranean storms that make it to Iraq reveals no discernible difference between the number of cyclones that occur during the NAO's positive and negative phases (rainfall was weak or heavy). The cyclones' varying intensities do exist, though (Khidher and Pilesjö, 2014). This phenomenon means that not all rainfall is necessarily accompanied by thunderstorms, but rather it depends on the type of cloud or the cloud formations associated with the low-pressure system as it passes over the region. Non-rainy thunderstorms are storms that have lightning and thunder but no rain because the clouds that produce them are not thick and have low relative humidity. They are caused by the production of medium and high clouds, which happens when the air is comparatively dry and stable (Humood and Abbas, 2017). In general, the climate record for thunderstorms at Khanaqin station does

not show a clear linear trend towards increasing or decreasing over the past three decades. This indicates that short- to medium-term climate fluctuations primarily govern the change in storm frequency. However, continued monitoring and analysis of thunderstorm data over longer times and linking it to factors such as surface humidity, lower atmospheric temperatures, and atmospheric pressure distribution may help clarify future trends in thunderstorm activity in the region. The Zagros Mountains act as a massive natural barrier that forces moist air masses coming from depressions (such as the Mediterranean and Red Sea depressions) to rise upward. This forced rise causes the air to cool and condense rapidly, stimulating the formation of violent cumulus clouds and thunderstorms, which explains the increased thundery activity at Khanaqin Station and border areas compared to the flat sedimentary plain. This area represents a unique "contact point" where the dry, cool air descending from the mountain highlands meets the warm, humid air settling over the Mesopotamian plain. This thermal and spatial variation creates severe atmospheric instability, making it a hotbed for violent thunderstorms, especially in the spring and fall. Khanaqin station is distinguished by its height exceeding 180 meters above sea level, so it records the highest number of thunderstorms compared to areas of lower height (sedimentary plain) or areas in the Mesopotamia plain, for example, Baghdad, where it recorded the lowest number of thunderstorms in 30 years (Al-Ansari, 2021; Ioshpa and Al-Khulaifawi, 2023). The Zagros Mountains direct the paths of depressions coming from the Mediterranean, forcing these depressions to settle longer over the interaction zone, increasing the number of "thunderstorm days" at stations such as Khanaqin compared to inland areas (WMO, 2024).

Statistical analysis using the Mann-Kendall test showed a statistically non-significant slight upward trend at a confidence level of 95%, which ranged between -0.111 and 0.286 in the number of annual thunderstorm days in the Khanaqin station during the period 1990–2019 ($Z = 0.69$, $P = < 0.05$). This indicates that the change observed in the graph may be the result of natural climate fluctuations rather than a radical medium-term shift. The Theil-Sen slope estimator indicated an increase of 0.08 days per year, which reflects a slight, gradual growth in thunder activity. The mean value was 19.2 thunder days per year, and the standard deviation was 5.7 days. The coefficient of variation was approximately 29.75%, which indicates a medium variation between years. This physical increase may be due to the following: Increase in relative humidity in the mid-latitude layers over Diyala Governorate (Khanaqin) and its greater exposure to mid-latitude depressions due to its height above sea level and the nature of its climate compared to the city of Baghdad, which recorded a lower frequency (Al-Khulaifawi and Mutar, 2026).

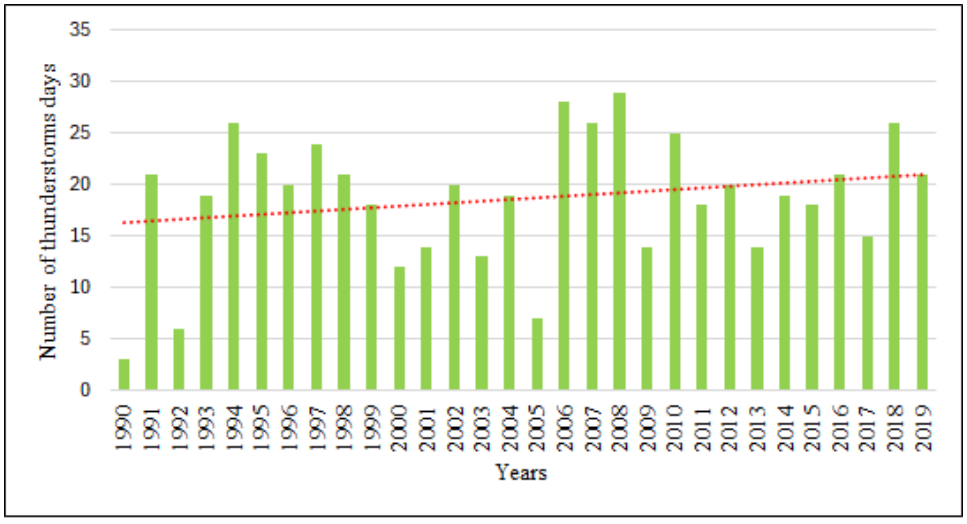


Figure 2. Annual thunderstorm distribution at Khanaqin station from 1990 to 2019

Figure 3 shows the monthly distribution of thunderstorm frequency recorded at Khanaqin station during the period from 1990 to 2019. Analysis shows that thunderstorm activity in the region is characterized by a distinct seasonality, with most storms concentrated during the spring and autumn, peaking in March and April (Al-Khulaifawi

& Ioshpa, 2025; Al-Khulaifawi and Mutar, 2026). The highest frequency of thunderstorms was recorded in April, with the number of cases exceeding 120 storms; this figure accounts for 22.86% of all frequencies (averaging 4.3 events per month) during the study period, followed by March with more than 100 storms. This total accounts for 18.75% of all frequencies (averaging 3.5 events per month), reflecting an increase in atmospheric instability rates during the spring months as a result of the intersection of cold air masses coming from the upper latitudes with warm, moist air masses from the lower latitudes. These conditions lead to enhanced convection and the formation of cumulonimbus clouds, which are responsible for thunderstorms. With 290 events, approximately ten thunderstorms each season, spring is the season with the highest frequency of thunderstorms, accounting for 51.79% of all frequencies (more than half of the total number).

On the other hand, no thunderstorms were recorded or observed during the summer season. In autumn, September is the least active month, with recorded storms numbering about 9. This phenomenon is attributed to the dominance of subtropical high-pressure systems during the summer months, which stabilize the atmosphere and prevent the development of cumulonimbus clouds. In October and November, there are 48 thunderstorm events (averaging 1.6) and 64 thunderstorm events (averaging 2.1), respectively. With 121 recorded thunderstorms, approximately four each season, autumn is the third most common season, accounting for 21.61% of all frequencies. Moderate thunderstorm activity is recorded as a result of the beginning of the decline of the thermal influence and the return of low-pressure systems passing through the region.

In winter, thunderstorms occur at moderate rates of 48–52 storms per month (averaging 8.57-9.29 events). There are 149 recorded thunderstorms throughout the winter, approximately five thunderstorms each season, accounting for 26.61% of all frequencies, reflecting some instability associated with cold fronts of mid-latitude lows. This distribution indicates that seasonal dynamics and thermal factors play the most important role in determining the pattern of thunder activity in Khanaqin, as spring is the most suitable period for storms to occur as a result of high surface temperatures, increased relative humidity, and the effectiveness of convection. The monthly distribution also shows a general consistency with the semi-arid climate patterns of the Diyala region, where the transitional seasons are characterized by more frequent weather disturbances compared to the stable seasons (summer and winter).

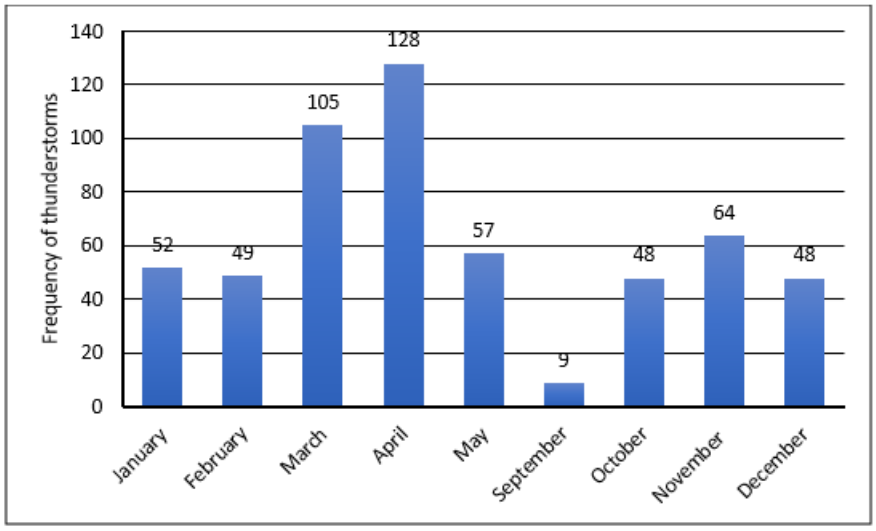


Figure 3. Monthly thunderstorm distribution at Khanaqin station from 1990 to 2019

One method for assessing the stability of the atmosphere at the moment is the use of atmospheric stability indices. The analysis of numerous numerical findings derived from atmospheric soundings acquired by radiosonde, satellite, etc., is the foundation for these indices (Gray et al., 1977; Leena et al., 2019; Madhulatha et al., 2013; Mathew et al., 2021; Ratnam et al., 2013). Figure 4 shows the K-index histogram for the period between 1990 and 2019 for thunderstorm events, which is calculated using an equation. The figure shows a clear variation in the frequency of

index values. The results indicate that the category between 26 and 30 represents the largest proportion of observations at (37.58%), followed by the category (31–35) at (26.93%). These values express medium to high levels of thermal and moisture instability in the atmosphere and are often associated with the formation of cumulus clouds. The concentration of the highest frequency ratios within the range (26–35) indicates that the atmospheric environment during the studied period was mostly characterized by conditions favorable to the development of moderate and intense convection, which is consistent with the climatic characteristics of the study area, which is exposed to frequent heat waves and periods of high relative humidity in the lower layers, creating suitable conditions for vertical instability. As for the categories with low values (K < 20), which amounted to 9.42%, they represent cases of atmospheric stability associated with the dominance of dry air masses, which limits the development of convection and reduces the chances of the formation of cumulus clouds. In contrast, very high values (K ≥ 40) that did not exceed 3.67% reflect rare cases of extreme instability, often associated with the passage of deep low-pressure systems or unusually humid tropical activity. These results indicate that the K index at the study station is mainly concentrated within the intermediate levels, meaning that thunderstorms are relatively frequent but mostly mild. This pattern is an important indicator in short-term weather forecasting, as its distribution can be used as a tool to estimate the probability of thunderstorms and assess the extreme nature of weather phenomena in the region. Furthermore, the change in the distribution of index values over time can help clarify the relationship between thermal and humidity activity and regional climate change over recent decades.

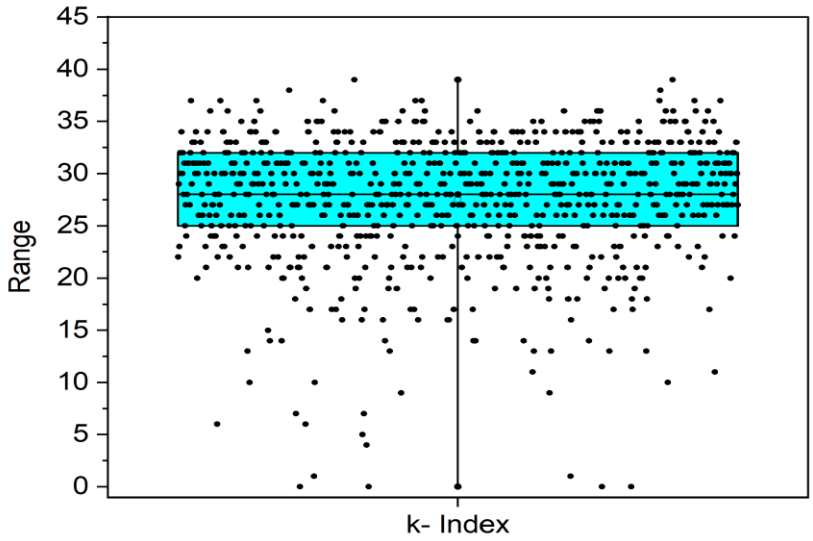


Figure 4. Statistical distribution of the K-index frequency values of thunderstorms at Khanaqin station for the period (1990-2019)

Figure 5 shows the frequency distribution of the Total Totals index for the period (1990–2019) for thunderstorm events, indicating that the category between 45 and 50 is the most frequent at 40.15%, followed by categories 51–52 and 53–56 at 25.46% and 21.54%, respectively. These values indicate the prevalence of moderate atmospheric instability in the region, as TT values within this range are usually associated with a sufficient thermal and humid environment for the development of cumulonimbus clouds and the occurrence of limited-intensity thunderstorms. The low categories (TT < 45), representing 10.77% of the cases, indicate relative atmospheric stability, while the very high values (TT > 57), accounting for 2.08% of the cases, reflect rare instances of extreme instability, which are often linked to strong thermal lifting processes or the passage of severe atmospheric depressions. Overall, this distribution shows that most of the study periods were characterized by moderately unstable conditions, making the TT index an effective tool for diagnosing thunderstorm activity and estimating the likelihood of atmospheric disturbances in the region. The results of the frequency distribution of both the K and TT indices for the period (1990–2019) showed that both clearly reflect the thermal and humid nature of the atmospheric layers in the study area, but there is a difference in the intensity of the response and the accuracy of representing instability conditions. K values

were concentrated between 26 and 35 (64.51%), while TT values were concentrated between 45 and 52 (65.61%), indicating that both indices accurately describe the dominance of moderate instability in the local climate. However, the K index is more closely related to the moisture content in the lower layers of the atmosphere and, therefore, more sensitive to changes in relative humidity and more effective in predicting short-lived local storms. The TT index, however, relies more heavily on the vertical temperature gradient between the 850 and 500 hPa layers, making it better able to represent large-scale disturbances and deep thunderstorms. Therefore, it is recommended to use both indices together for a more accurate assessment of atmospheric instability levels and to predict thunderstorm activity in the region. The results of the analysis of the K-Index and Total Totals Index (TT) indicate that the atmospheric climate over Iraq during the period (1990–2019) was characterized by a high frequency of moderate instability, with a scarcity of severe cases, which means a transitional nature of the atmosphere between near-permanent stability during periods of drought and limited instability during the transitional and spring seasons. This distribution reinforces the hypothesis that regional climate change has led to a redistribution of thermal energy and moisture characteristics in the lower layers of the atmosphere so that periods of atmospheric disturbance have become more frequent but less intense. Long-term monitoring of these two indicators would provide a scientific basis for developing early warning systems and improving the accuracy of thunderstorm forecasts in the region. There has been a notable upward trend in the TTI and KI indices with thunderstorm events over the Kerala region of India (Umakanth et al., 2024).

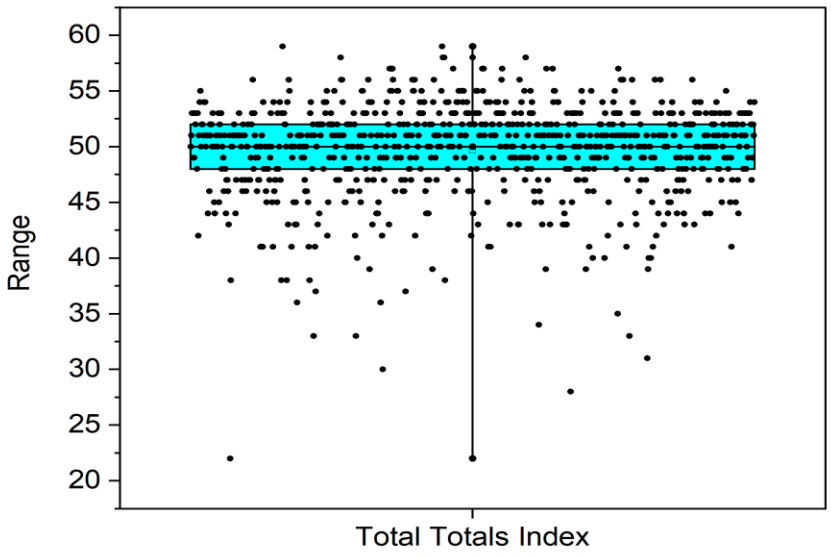


Figure 5. Statistical distribution of the Total Totals index frequency values of thunderstorms at Khanaqin station for the period (1990-2019)

Figure 6 illustrates the relative frequency distribution of the available convective potential energy (CAPE) within different categories for the time period from 1990 to 2019 for thunderstorm events, which is a fundamental analysis for understanding atmospheric stability and the potential for thunderstorm development in the study area. The data indicate a prevalence of relatively stable or weak convective weather conditions, with a limited increase in the potential for severe storms. The data show that the vast majority of CAPE parameter frequencies fall within the following categories:

• CAPE below 300: This is the most common category, representing 50.92% of all observations. This range of very low values indicates stable or very stable atmospheric conditions, where the upward buoyancy is insufficient to support the development of strong thunderstorms. This translates into a significant absence or weakness in convection and supports the presence of a strong convective inhibition (CIN) layer or insufficient heat in the surface layers.

• CAPE 300 to 999 category: This category represents the second most frequent occurrence, at 28.64%. These values are usually classified as weak to moderate convection energy and indicate the possibility of some cumulonimbus clouds or moderate thunderstorms, but they are not intense enough to generate violent weather phenomena. The sum of these two categories is approximately 79.56%, which confirms that the atmospheric cover of the region was, for most times (during the study period), either stable or with a low susceptibility to convection.

• CAPE 1000 to 2500 category: This category represents a frequency of 17.50%. These values are considered medium to high and indicate the possibility of strong thunderstorms accompanied by heavy rainfall and possibly small hail. This category represents most of the weather events that could be considered "storms" in the region. The frequency decreases sharply as the CAPE value increases, reflecting the rarity of extreme instability conditions.

• CAPE category 2500 to 3500: 1.96% is a minimal percentage. This range denotes extremely hazardous circumstances that significantly raise the probability of violent thunderstorms. Higher classifications indicate strong convective energy and the possibility of extreme weather events (supercells).

• CAPE category > 3500: This is the least common of all, at 0.98%. These extremely high values indicate the possibility of very violent and rare weather phenomena, such as massive hail or tornadoes, and confirm that these phenomena are exceptional events in the region.

Thunderstorm Activity at Istanbul Airport: During thunderstorm events, the K and total totals indices are well represented, and the convective available potential energy (CAPE) values, which are frequently utilized for atmospheric instability, are low (Kolay et al., 2025).

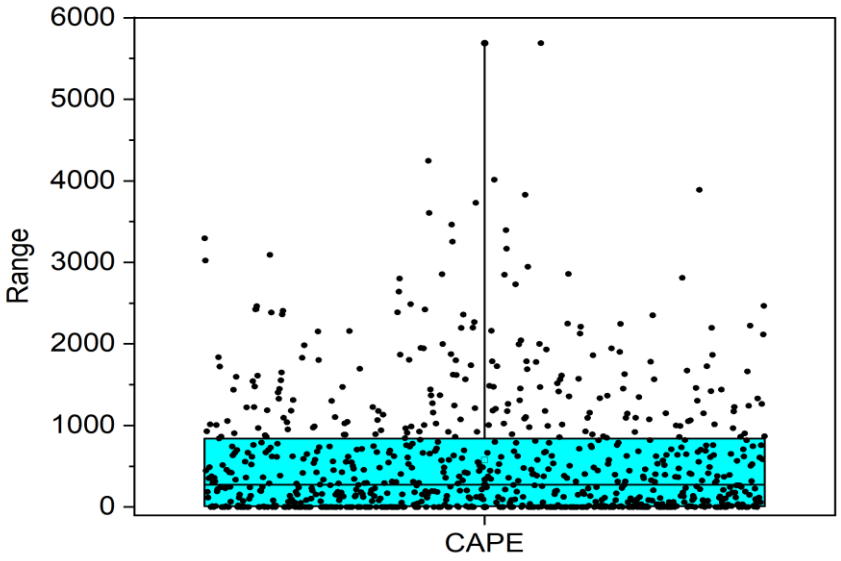


Figure 6. Statistical distribution of the CAPE parameter frequency values of thunderstorms at Khanaqin station for the period (1990-2019)

The study focused on thermodynamic indicators (heat and humidity) being the primary driver in semi-arid environments, recognizing that future studies should include shear-aware indices such as STP and EHI to better understand the dynamics of severe storms in the Zagros region. Descriptive statistical data details of indices and parameter CAPE at Khanaqin station for the period (1990-2019) are shown in Table 4. Seasonal distributions of the KI and TTI received their highest average value in spring (29.62% and 49.94%) and lowest in autumn (24.79% and 49.51%). While CAPE received its highest average value in winter (774.6%) and lowest in autumn (170.1%). The annual average values at the stations of the KI, TTI, and CAPE were 27.48, 49.66, and 576.26, respectively. Extreme

values of the KI, TTI, and CAPE were recorded in spring, reaching 39ºC, 59ºC, and 5688J/Kg, respectively. The peak of thunderstorms in Iraq during the spring (especially March and April) is a climatic phenomenon linked to the nature of the transitional season and the convergence of different atmospheric pressure systems. Severe atmospheric turbulence occurs when the Red Sea depression coming from the south, laden with humidity and heat, meets the Mediterranean depression coming from the north and west; this meeting leads to the formation of massive cumulus clouds, causing lightning, heavy rain, and hail. Spring is characterized by the alternation of cold polar air masses with warm tropical air masses, which creates a state of extreme atmospheric instability as a result of large thermal differences in the different layers of the atmosphere. With the onset of spring, solar radiation becomes more powerful, rapidly heating the Earth's surface. This stimulates convection processes that lift warm, moist air upward to collide with cold air in the upper layers, generating thunderstorms (Al-Khulaifawi & Ioshpa, 2025; Al-Khulaifawi and Mutar, 2026).

Table 4: Data details of thermodynamic atmospheric stability indices and parameter CAPE for the period 1990–2019 over Khanaqin station.

	N total	Mean	Standard deviation	Sum	Minimum	Median	Maximum	Best season	lowest season
k-Index	817	27.48	6.03	22452	0	28	39	29.62%	24.79%
Total Totals Index	817	49.66	4.31	40573	22	50	59	49.94%	49.51%
CAPE	817	576.26	762.79	470812	0	275	5688	774.6	170.1

4.2. Analysis and Evaluation of the Correlation Coefficient Between Temperature, LCL, EL, Thickness, and Atmospheric Stability Parameter (CAPE) for Thunderstorm Events

Elevated surface air temperature is a major factor in increasing atmospheric instability, leading to an increase in available latent convective energy (CAPE), the energy that fuels and develops thunderstorms. Surface heating raises the temperature of air parcels near the surface, which decreases their density and provides the necessary acceleration for them to begin floating in the atmosphere; as a result, they rise to higher layers where they can release their latent energy through effective convection. This indicates that surface temperature is the primary factor in initiating and sustaining thermal instability, as it directly controls the amount of energy available for convection.

The results show a relatively strong positive relationship between surface temperature (T) and the lifting condensation level (LCL), with a correlation coefficient of R = 0.7, in Figure 7, indicating that a rise in surface temperature leads to a rise in the level of condensation in the atmosphere. The empirical equation for linear regression (LCL = -346.93 + 99.74*T) expresses this relationship, indicating that every 1°C increase in surface temperature corresponds to an increase of approximately 99.74 meters in the height of the condensation level. This behavior is attributed to the fact that a higher surface temperature increases the air's ability to hold water vapor, leading to a decrease in relative humidity and a move away from a state of saturation. As a result, the air needs to rise to higher levels to cool and reach the dew point, that is, the point at which actual condensation begins. This phenomenon explains the marked increase in LCL values with rising temperature. As can be seen in the figure, the dispersion of data points around the regression line indicates that the relationship is also influenced by other factors, such as the actual amount of water vapor in the surface layer and daily variations in terrestrial heating and radiation, as well as local surface characteristics (soil moisture and vegetation cover). However, the high correlation strength (R = 0.7) confirms that surface temperature remains a key and direct factor in determining the height of the condensation level. In general, this relationship reflects that hot, dry conditions lead to a higher condensation level (LCL), which reduces

the likelihood of low cloud formation, while cold, humid conditions lower the LCL and increase the chances of vapor condensation and cumulus cloud formation. Rising surface temperature increases the saturation deficit in the near-surface layers, pushing the condensation level (LCL) to higher levels, a pattern prevalent in semi-arid regions as a result of strong sensible heating (Markowski and Richardson, 2010). The findings demonstrate that compared to surface-based LCL heights, the mean error for mean-layer LCL heights was significantly lower. These results imply that the mean-layer parcel is probably a better representation of the real parcel linked to convective cloud formation, which has consequences for the computation of thermodynamic parameters like convective inhibition and available convective potential energy (Craven et al., 2002).

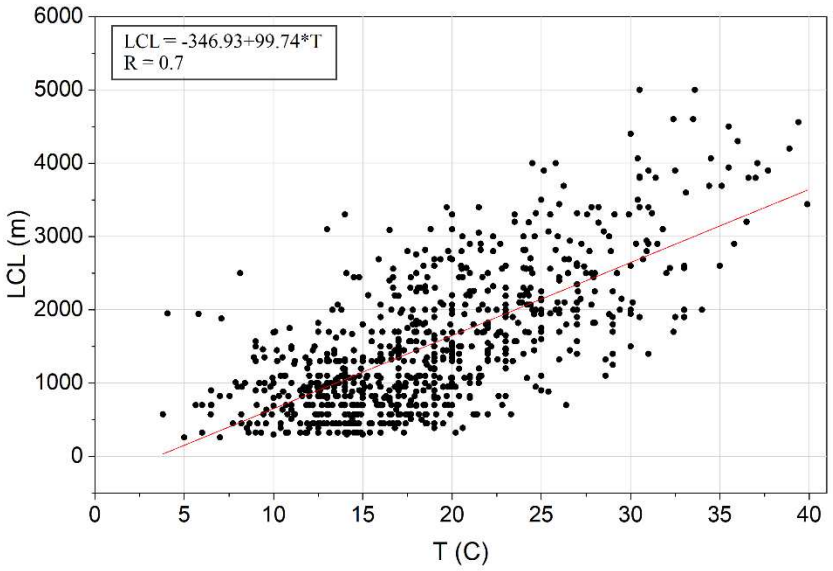


Figure 7. Correlational relationship between surface temperature and lift condensation level at Khanaqin station for the period (1990-2019)

The relationship between temperature and equilibrium level, as shown in Figure 8, was analyzed using a linear regression model. The data show a clear positive linear correlation between them (R = 0.7). That is, the temperature rise is associated with an increase in the height of the equilibrium level in the atmosphere, which is consistent with the thermodynamic principles that link the heating of the lower layers (high temperatures) with the rise in equilibrium levels. Despite the clear positive trend, the graph points show a large dispersion around the red regression line, especially in the middle temperature range (10°C to 30°C). This dispersion indicates that the strength of the correlation is moderate and that temperature, although an important factor, does not alone explain the entire variance in the equilibrium level, indicating the intervention of other atmospheric factors (humidity content, wind shear, and vertical changes in the atmosphere) in predictive models to increase the accuracy of explaining the variance in the equilibrium level. This is because surface heating raises the temperature of air parcels near the surface, which leads to a decrease in their density and gives them the necessary acceleration to begin the process of floating within the atmosphere, and thus they rise to higher layers, where they can release their latent energy in the form of effective convection. The empirical equation for linear regression (EL = 4023.4 + 239.5*T) shows that every 1°C increase in temperature theoretically leads to an increase in the equilibrium level of 239.5 m, with a predicted value exceeding 12,000 m at higher temperatures. Indicates that surface temperature is the primary factor in the initiation and maintenance of thermal instability. It is well known that convective cloud features vary greatly across different regions and are influenced by the underlying surface's topography, atmospheric temperature and humidity profiles, and atmospheric circulation patterns. Clarifying the convective cloud parameters that cause dangerous convective phenomena in various geographic locations will therefore enhance regional weather prediction methods and advance knowledge of the physical processes occurring in such clouds during hail and thunderstorm formation. The following

factors are of special importance to study the dangerous occurrences generated by convection and develop promising methods for their prediction: the top cloud height and atmospheric convective potential energy, which are constrained by the equilibrium level (EL), also known as the level of neutral buoyancy (LNB), and the degree of free convection in the studied region (Sinkevich et al., 2016; Ye et al., 1998).

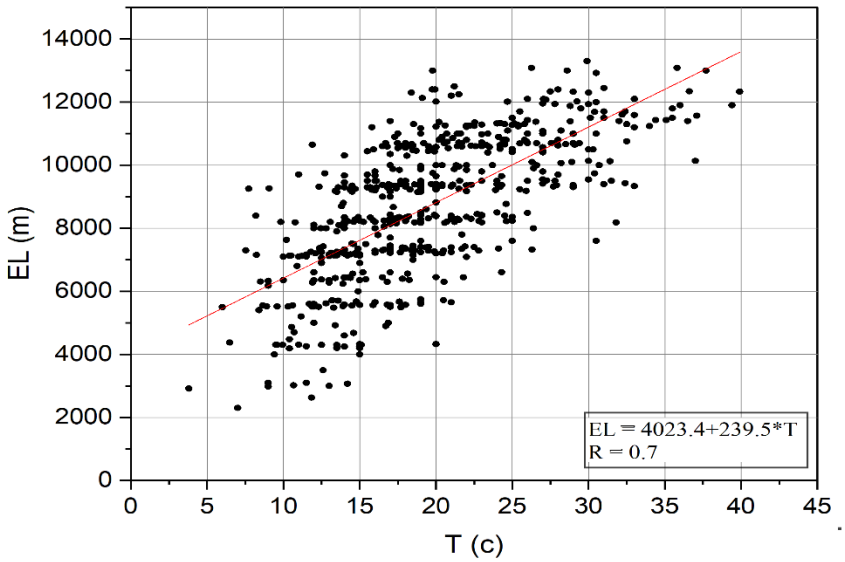


Figure 8. Correlational relationship between surface temperature and equilibrium level at Khanaqin station for the period (1990-2019)

From Figure 9 (values of CAPE equal to zero have been removed; there is no data for the equilibrium level), the data indicate a positive and nonlinear correlation (R = 0.7) between the convective available potential energy (CAPE) and the equilibrium level (EL). This relationship was plotted using an exponential growth model (ExpGro1). As the CAPE value increases, the equilibrium level (EL) also increases. The equilibrium level increases sharply and rapidly at low and medium CAPE values (less than about 2000 j/kg), but then the curve begins to saturate or flatten at higher CAPE values. This indicates that the effect of increasing CAPE on raising the equilibrium level becomes less pronounced after a certain limit, and the equilibrium level approaches an approximate maximum value. The value of the adjusted coefficient of determination (R-square) of 0.7 confirms that the exponential model is suitable for representing the data distribution and provides excellent predictive power, although there are scattered points with high dispersion, especially at CAPE values exceeding 2000 J/Kg. This analysis confirms the important role of CAPE as a catalyst for convection and its direct relationship to the maximum height of deep convective clouds.

From Figure 10 (values of CAPE equal to zero have been removed; there is no data for thickness), the data clearly indicate a strong and nonlinear positive correlation (R = 0.6) between the convective available potential energy (CAPE) and thickness. Using a double exponential model (ExpGro1), the layer thickness increases as the CAPE value increases. This increase is more pronounced and rapid at lower CAPE values (below approximately 1000 J/Kg). As CAPE continues to increase, the curve begins to flatten (saturate), indicating that the effect of subsequent CAPE increases on layer thickness becomes less significant at higher values. The graphs exhibit a noticeable dispersion, particularly at high CAPE values, despite the strong correlation. This dispersion suggests that CAPE is not the sole factor influencing layer thickness and that other atmospheric factors play a significant role in the remaining variation. This indicates that surface temperature is the primary factor in initiating and sustaining thermal and atmospheric instability. Thickness values help to define the boundaries between warm and cold air masses; thickness lines accumulate at air fronts. The thickness of the layer is an important indicator for predicting whether precipitation will be in the form of rain, snow, or freezing rain, because this value reflects the average temperature in the lower layers

of the troposphere (and the troposphere naturally varies between regions). High CAPE values result from a hot air mass with a thickness of 1000–500 mb. These air masses can create small or large hailstones, or they can produce heavy rain instead of hailstones (Laura et al., 2001).

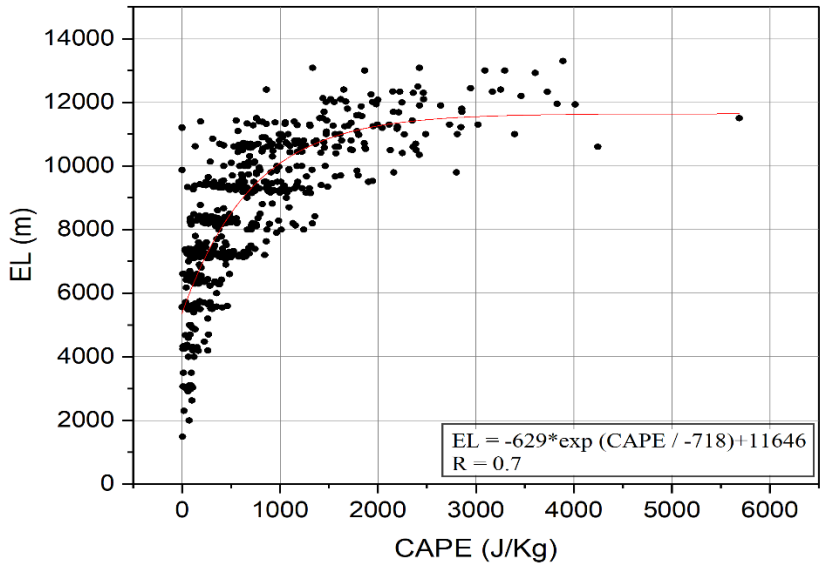


Figure 9. Correlational relationship between CAPE and equilibrium level at Khanaqin station for the period (1990-2019)

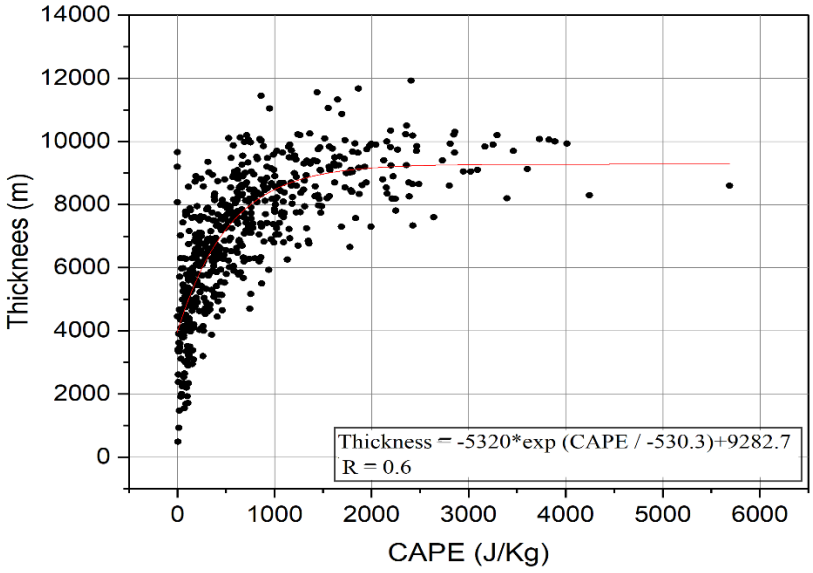


Figure 10. Correlational relationship between CAPE and thickness at Khanaqin station for the period (1990-2019)

Tables 5 and 6 show statistical relationships using linear and non-linear/exponential growth (ExpGro1) models. Temperature (T) had strong, significant linear correlations with thermal lift (LCL) and equilibrium level (EL) (R = 0.7, P-values = 0.0001–0.0004). CAPE showed a strong exponential relationship with EL (R^2 = 0.7, P = 0.0004) and thickness (R^2 = 0.6, P = 0.0005).

Table 5: Results of the regression analysis of the linear relationship between the selected variables.

Variables (Relationship)	Model	a	b	R	R^2	P-value
T and LCL	Linear	- 346.93	99.74	0.7	0.5	<0.0004
T and EL	Linear	4023.4	239.5	0.7	0.5	<0.0001

Table 6: Results of the regression analysis of the exponential growth relationship between the selected variables.

Variables (Relationship)	Model	A_1	t_1	Y_0	R	R^2	P-value
CAPE and EL	ExpGro1	-629	-718	11646	0.7	0.7	<0.0004
CAPE and Thickness	ExpGro1	-5320	-530.3	9282.7	0.6	0.6	<0.0005

5. Synoptic Analysis

Figure 11 shows the relative distribution of synoptic system types associated with thunderstorm occurrences at Khanaqin station during the period 1990–2019 and for six months of the year (March, April, May, September, October, and November). The results show that shallow mid-latitude depressions accounted for the largest proportion of impactful cases at 53.13% of the total depressions, while deep mid-latitude depressions accounted for 46.88%. This distribution indicates that most thunderstorms in the Khanaqin region are generated under the influence of relatively shallow atmospheric systems, reflecting the transitional climatic nature of the region, which lies between the semi-arid climate of central Iraq and the semi-humid climate of the eastern mountainous regions. It can be concluded that the continued dominance of shallow depressions by a small percentage over the past three decades may reflect a gradual shift, like climatic influences, towards more pronounced local thermal patterns, which is consistent with regional climate change indicators that point to rising temperatures and declining atmospheric humidity in Iraq. To improve thunderstorm forecasting systems and lessen their impact on agricultural and urban operations in Diyala Governorate and surrounding areas, this shift emphasizes the necessity for a long-term dynamic investigation of the weather systems influencing the region.

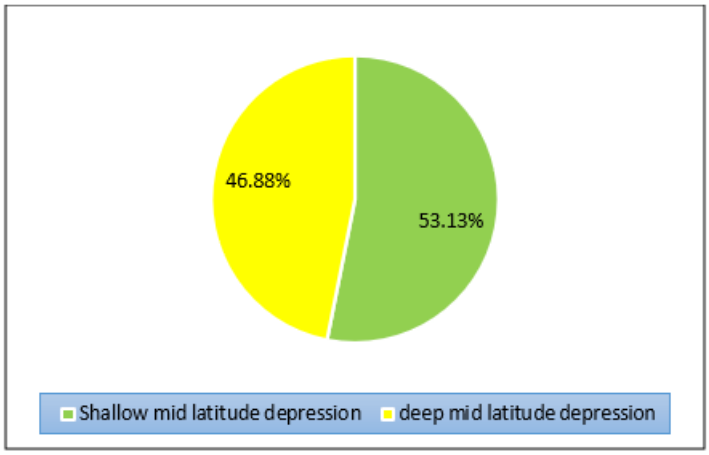


Figure 11. The relative distribution of Shallow and Deep mid-latitude depressions at Khanaqin station for the period 1990-2019

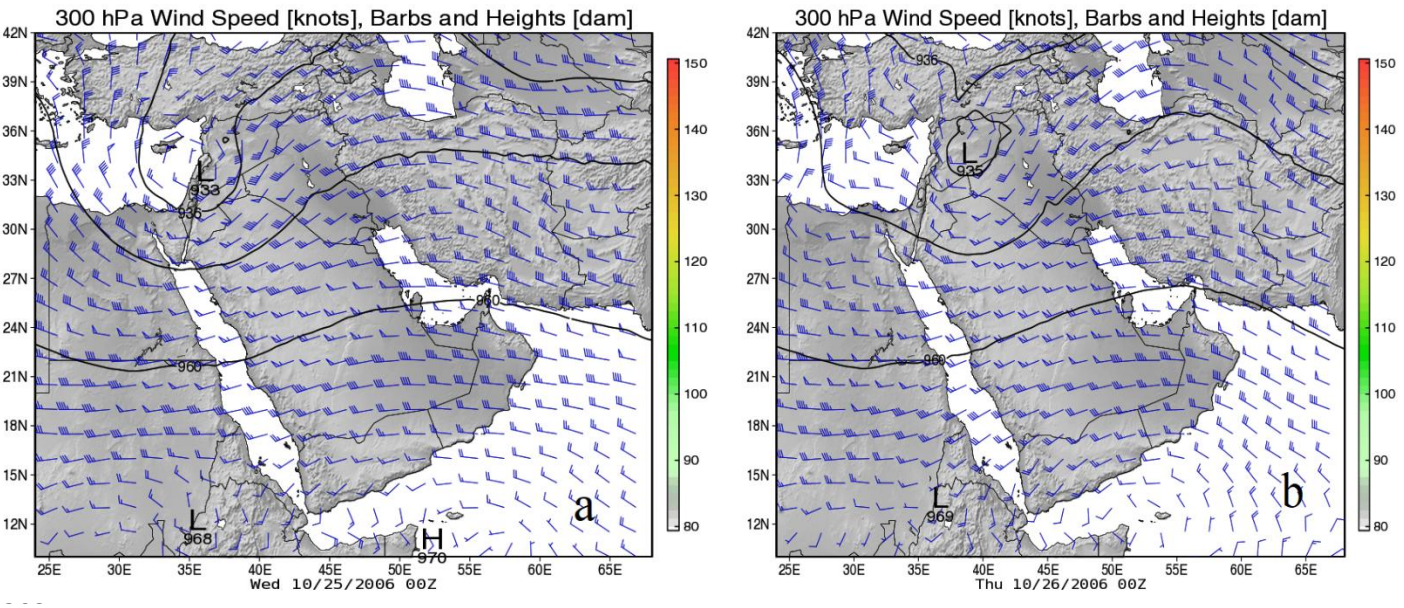
5.1. Case Study

Thunderstorm events were identified based on daily surface observations from the Khanaqin meteorological station. A thunderstorm day can be defined as any day with a reported thunder occurrence in the synoptic records. Thunderstorm days are a key climate indicator for assessing atmospheric electrical activity in a given area. According to international standards issued by the World Meteorological Organization, the sound of thunder is heard at least

once within 24 hours, regardless of whether rainfall or lightning is seen with the naked eye, at a meteorological station or its surroundings within a range of 10–15 kilometers (WMO, 2024). With incomplete surface observations, days were excluded to ensure data consistency. All identified events were treated with equal weight in the statistical analysis. Thunderstorm events were analyzed using data observed from the Khanaqin weather station at 00:00, 06:00, 12:00, and 18:00 local time for each thunderstorm; as for the upper data, it was analyzed using MERRA-2 to include wind speed and direction, geopotential height at the level of 300, temperature, geopotential height at the level of 500, and LCL convective available potential energy. This analysis covered the cases of shallow and deep depressions in the mid-latitudes and is considered one of the exceptional cases in which thunderstorms continued to be recorded for several separate hours with moderate-heavy precipitation for some observations. Atmospheric stability indices were recorded, such as the K index exceeding 35°C, the Total Totals index exceeding 53°C, and the CAPE parameter exceeding 1500 J/kg.

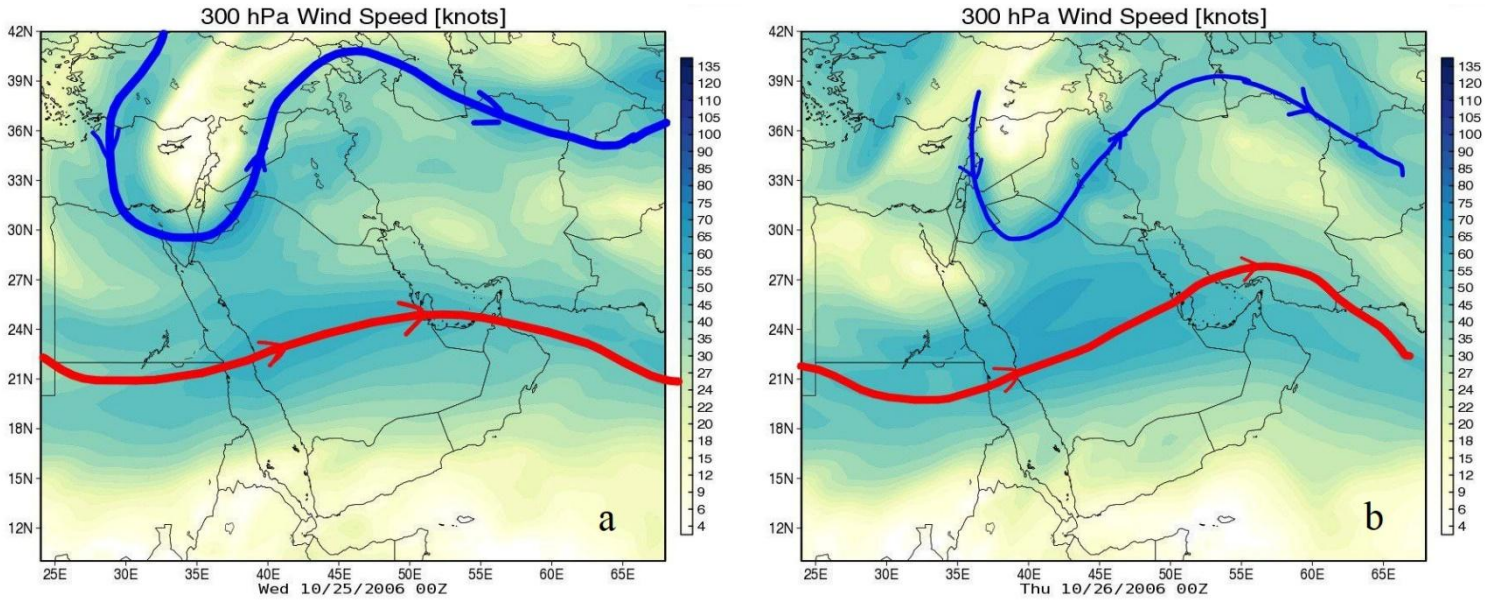
5.1.1. Thunderstorm Case of October 25 and 26, 2006 (Shallow Mid-Latitude Depression)

The results of the analysis based on 300 hPa maps (Figures 12 and 13) show that the studied case is a clear example of the crucial role jet streams play in organizing and activating deep atmospheric disturbances over the Middle East, particularly eastern Iraq. In Figure 12 (a–b), strong upper-level winds with a clear gradient in speed and direction are evident, indicating a dynamically active upper troposphere environment conducive to generating large-scale upper-level divergence. Investigated the relationship between vertical velocities and cloud and precipitation properties, as well as condensation and freezing processes within moisture-bearing and cumulonimbus clouds. The results show that moderate to strong updrafts (>3–5 m/s) are responsible for the majority of cloud condensation and freezing, while strong updrafts (>10 m/s) contribute to the development of the upper cloud portion and the ice formation and dispersal phases (Tao et al., 2022). Figure 13 (a–b) clearly shows two distinct jet stream paths. The blue path represents the polar jet stream extending from higher latitudes toward the Middle East, while the red path represents the subtropical jet stream extending from North Africa and the Arabian Peninsula. It is noteworthy that eastern Iraq, including the city of Khanaqin, lies within the interaction or coupling zone of these two jet streams, an area known dynamically to be one of the most active in generating upper-level divergence and forced updrafts. From a dynamic perspective, the overlap of the polar jet stream's right entrance region with the subtropical jet stream's left exit region leads to a significant enhancement of divergence at upper levels, consistent with classical jet theory. This divergence contributes to the removal of air mass from the top of the atmospheric column, resulting in lower pressure and driving sustained vertical uplift. This upper-level structure aligns with the findings from the lower and middle levels of the study, where the upper-level lift resulting from the jet stream coupling capitalizes on pre-existing thermal instability in the lower layers. Thus, the polar jet stream plays a key role in introducing cold air and increasing vertical wind shear, while the subtropical jet stream helps maintain a flow of warm, moist air from lower latitudes, creating an ideal environment for the development of deep and organized thunderstorms. These results indicate that the thunderstorms experienced in Khanaqin were not the product of limited local development, but rather a direct response to a large-scale synoptic mechanism controlled by jet stream interaction. This conclusion is reinforced by the climatological literature, which confirms that the coupling of the polar jet stream with the subtropical jet stream is one of the most effective mechanisms for generating extreme weather, particularly in climate transition and semi-arid regions (Holton and Hakim, 2013; Markowski and Richardson, 2010). The subtropical jet stream affects the 300 hPa layer over Iraq more quickly than the polar jet stream, and there is a significant degree of consistency in the change in temperature and pressure values between the two. That is, the temperature and pressure values rise and fall at the same time, but there isn't a significant time difference over the course of the study between January 26, 2024, and February 9, 2024 (Hussain et al., 2025).



564 **Figure 12.** Wind speed (knots) and direction and geopotential height (dam) at 300 hPa: (a) October 25,
565 2006; (b) October 26, 2006

566 - The blue path represents the polar jet stream, and the red path represents the subtropical jet stream in Figure 13
567 (a–b).



569 **Figure 13.** Wind speed (knots) and jet stream paths at 300 hPa: (a) October 25, 2006; (b) October 26, 2006

570 Figure 14 (a to b) shows the evolution of temperature and potential height distributions at the 500 hPa level
571 over the Middle East region during two consecutive 24-hour periods, based on MERRA-2 data. The 500 hPa level is
572 a key reference level in synoptic analysis, as it reflects the average thermal and dynamic structure of the atmosphere
573 and clearly shows the positioning of troughs and upper-level highs associated with the development of weather
574 systems. In the first map, Figure (14a), a clear upper-level trough is observed centered over the eastern Mediterranean.
575 The southerly bending of potential height lines and their declining values to roughly 570 dams are indicative of the

trough. Alongside this phenomenon, comparatively cold air spreads to lower latitudes, where northern parts see temperatures as low as -20°C. This pattern indicates a state of relative instability in the mesosphere, resulting from the deepening of the trough and the increasing horizontal temperature gradient between the cold air masses to the north and the warm air masses to the south. In contrast, the southern regions of the Arabian Peninsula show the dominance of a subtropical upper-level high, characterized by potential height values reaching 586–587 dams, accompanied by relatively higher temperatures. This thermo-potential contrast reflects the presence of an active baroclinic transition zone separating the two systems, an area often considered conducive to the development of medium-scale atmospheric disturbances. After 24 hours, Figure 14b, the results show a clear dynamic change in the structure of the thermo-potential fields. An eastward shift of the upper-level trough is observed, with a slight tendency toward flattening, accompanied by a relative increase in potential height values over the eastern Mediterranean and the Levant, indicating the beginning of a weakening of the upper-level cold air influence. Simultaneously, the subtropical high strengthens over the Arabian Peninsula, with potential height values rising to around 588 dams, accompanied by a more pronounced northward extension of warm air. The maps also show a narrowing of the horizontal temperature gradient compared to the previous day, indicating a decrease in the intensity of the baroclinic activity in the region. This development indicates a transition of the atmospheric system from a dynamically active phase to a relatively more stable one, particularly in the mid-atmosphere. This change is likely related to the eastward advance of the upper-level trough and its diminishing direct influence on the studied region. From a physical perspective, the observed changes over the 24 hours reflect the ongoing interaction between horizontal thermal advection and the evolution of short-wavelength planetary waves. They also underscore the crucial correlation between temperature and potential height at the 500 hPa level in determining the trajectories and temporal evolution of atmospheric systems.

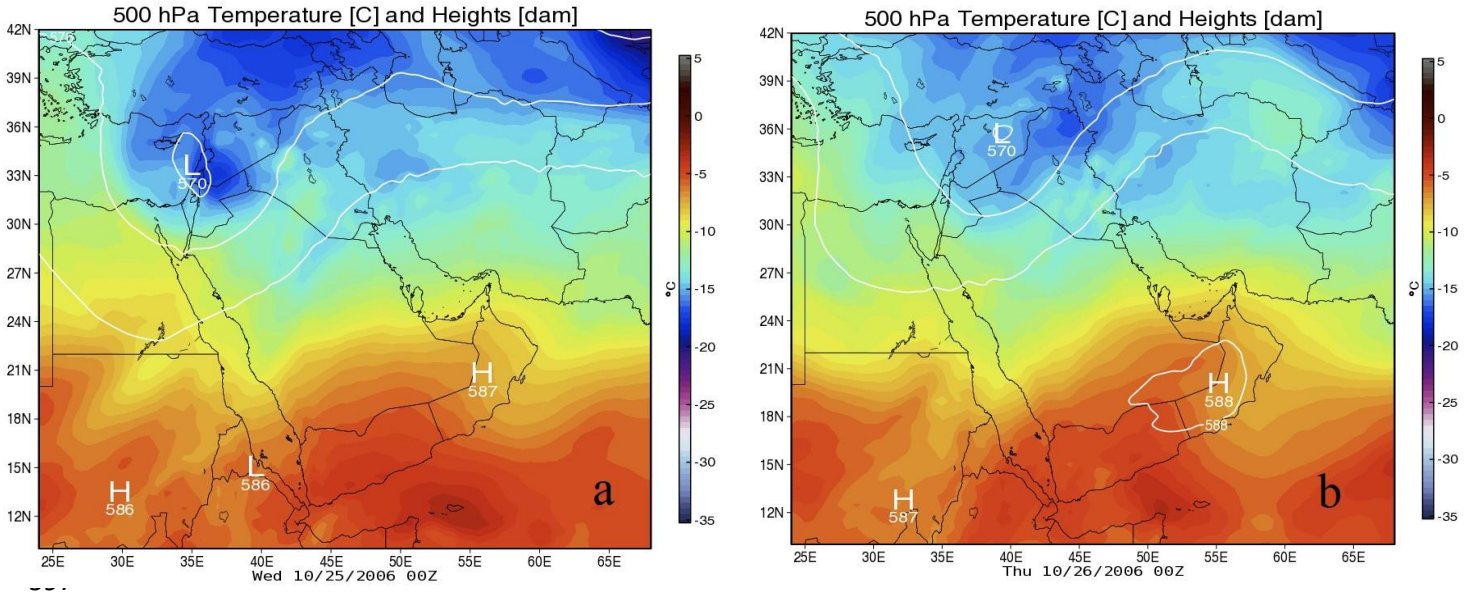


Figure 14. Air temperature (°C) and geopotential height (dam) at 500 hPa: (a) October 25, 2006; (b) October 26, 2006

Figures 15 (a to c) illustrate the temporal evolution of temperature distribution at a height of 2 meters over the three days (October 25, 26, and 27) across the Middle East. This type of temporal analysis is a crucial tool for distinguishing between thermal changes resulting from local processes and those associated with the movement of large-scale air masses. On the first day, the map shows the dominance of relatively warm air over most of the Arabian Peninsula and Iraq, with relatively high and uniform surface temperatures. Cooler air is located in the north over Anatolia and the eastern Mediterranean. A horizontal temperature gradient is evident along a latitudinal band extending from the Eastern Mediterranean to northern Iraq and Iran, indicating a transition zone between two air

masses with contrasting thermal characteristics. On the second day, an advection of the cold air mass to the north can be observed, extending southward towards northern Syria and northern Iraq. This is accompanied by a noticeable drop in surface temperatures in these areas compared to the previous day. This expansion coincides with the southeastward movement of the thermal gradient, a typical behavior of the frontal advance phase, where colder air begins to displace the less dense warm air over a wide horizontal area. On the third day, the maps show the continuation of this temporal development. The thermal gradient firmly establishes the colder air mass behind it, stabilizing relatively low temperatures in the northern regions. The warm air continues to dominate the southern and southeastern parts of the Middle East. This pattern indicates the completion of the frontal transit phase, with the front moving further south or eastward and the post-frontal stage beginning. For Iraq, the arrival of cold air stopped in the west and north of the country. The impact of the baroclinic instability resulted from upper-level cold troughs, which extended to central, southern, and eastern Iraq; thus, the cold front was in a frontolysis stage. In Khanaqin, eastern Iraq, the primary influence was upper-level cooling, meaning the mid-latitude depression impact was shallow and did not deepen due to the frontolysis of the cold front in western Iraq.

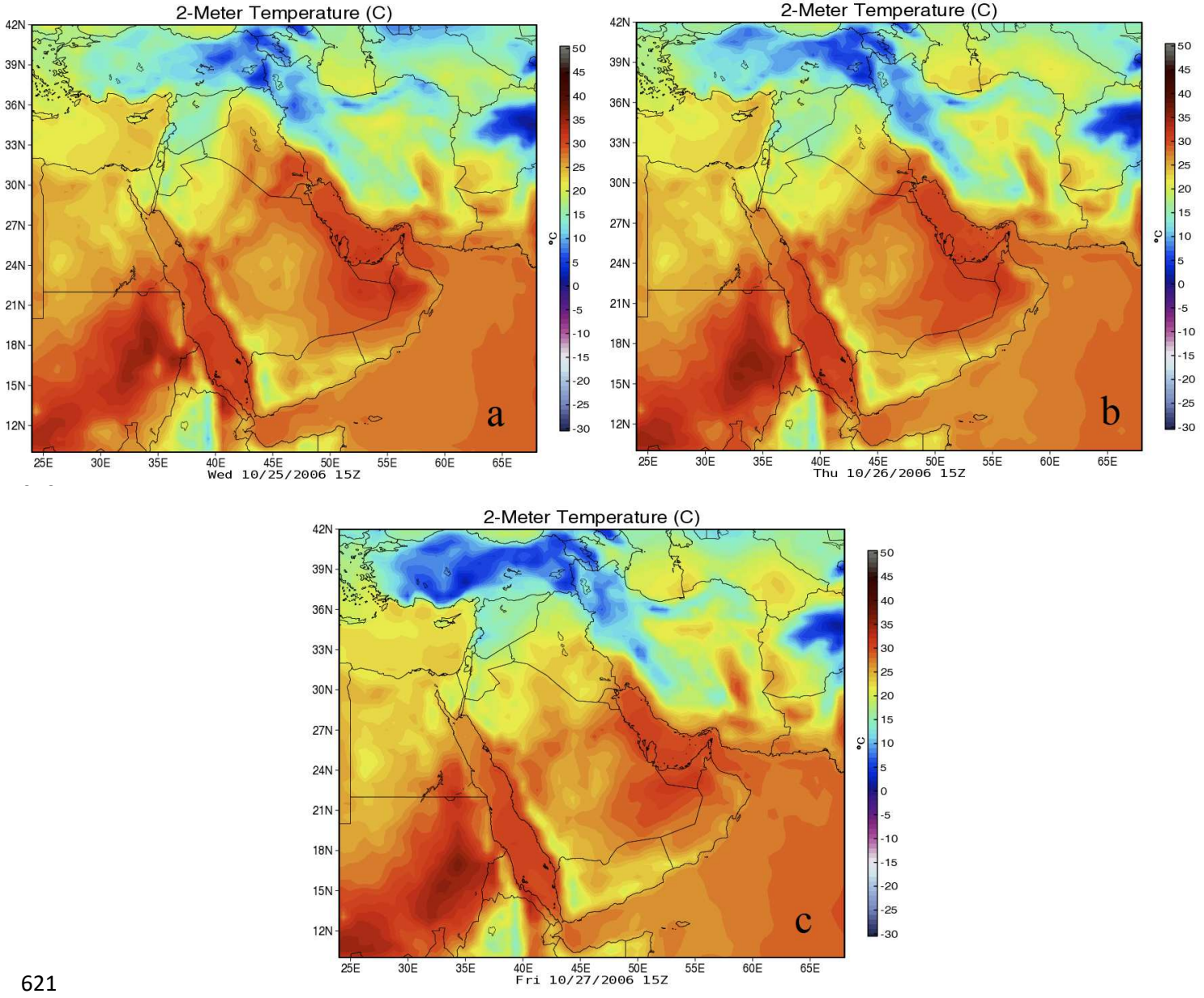


Figure 15. Air temperature distribution (°C) at a height of 2 meters: (a) October 25, 2006; (b) October 26, 2006; (c) October 27, 2006

Figure 16 presents a composite analysis of the weather conditions that affected Khanaqin on October 25, 2006, by combining atmospheric sounding data (Figure 16a) with satellite imagery of cloud tops (Figure 16b).

Figure 16a shows the thermal and dynamic analysis from the skew-T log P chart. The sounding data reveal a thermal instability in the lower and middle atmospheric layers, manifested by the following:

- The ambient temperature curve converges with the air parcel temperature curve and even exceeds it in some layers.
- The presence of significant positive values for the available convective potential energy (CAPE), totaling 3288 J, indicates that air masses can rise freely after exceeding the level of lift condensation (LFC).
- Wind direction and speed exhibit a significant vertical wind shear, particularly between near-surface and mid-level and upper-level atmospheric conditions. This shear is a key element in regulating convection and preventing the rapid collapse of updrafts, allowing for the development of deep and relatively well-organized cumulonimbus clouds.
- Furthermore, the diagram does not show a strong capping inversion layer impeding the updraft, indicating that the available dynamic lifting mechanisms were sufficient to initiate convection.

On the other hand, Figure 16b, a satellite image of cloud top temperature (CTT), shows cold cloud tops over Khanaqin and surrounding areas, with CTT reaching approximately -70°C, indicating cloud extension into the upper atmosphere (more than 12 km in height). This pattern is characteristic of cumulonimbus clouds, which are accompanied by heavy rainfall and electrical activity. It is also the cloud distribution that is not random but rather forms a quasi-linear band or cluster of cells, indicating an influence of large-scale dynamic factors, such as upper-level lift associated with divergent zones in the upper atmosphere, particularly at the 300 hPa level, as noted in previous analyses.

When these results are linked to the previously analyzed jet stream development, upper-level troughs, and surface cold fronts, it becomes clear that the weather pattern over Khanaqin resulted from a complex vertical interaction between:

- Thermal instability in the lower layers,
- Upper-level dynamic support is provided by upper-level divergence associated with the jet stream.
- This includes a surface-level forced lift mechanism that is connected to the topography of eastern Iraq near Khanaqin.

This synchronization of thermal and dynamic factors explains the intensity of cloud development and its high depth, as illustrated by both satellite imagery and sounding data. From a physical perspective, this phenomenon can be classified as a synoptically forced convection pattern, where cloud development depends not only on surface heating but is primarily enhanced by large-scale dynamic lift. This type of pattern is common in subtropical regions during transitional seasons, particularly when cold upper-level air interacts with warm, moist lower-level air.

- The blue line represents the dew point temperature, the black line represents the environment temperature, and the red line represents the CAPE value in Figure 16a.

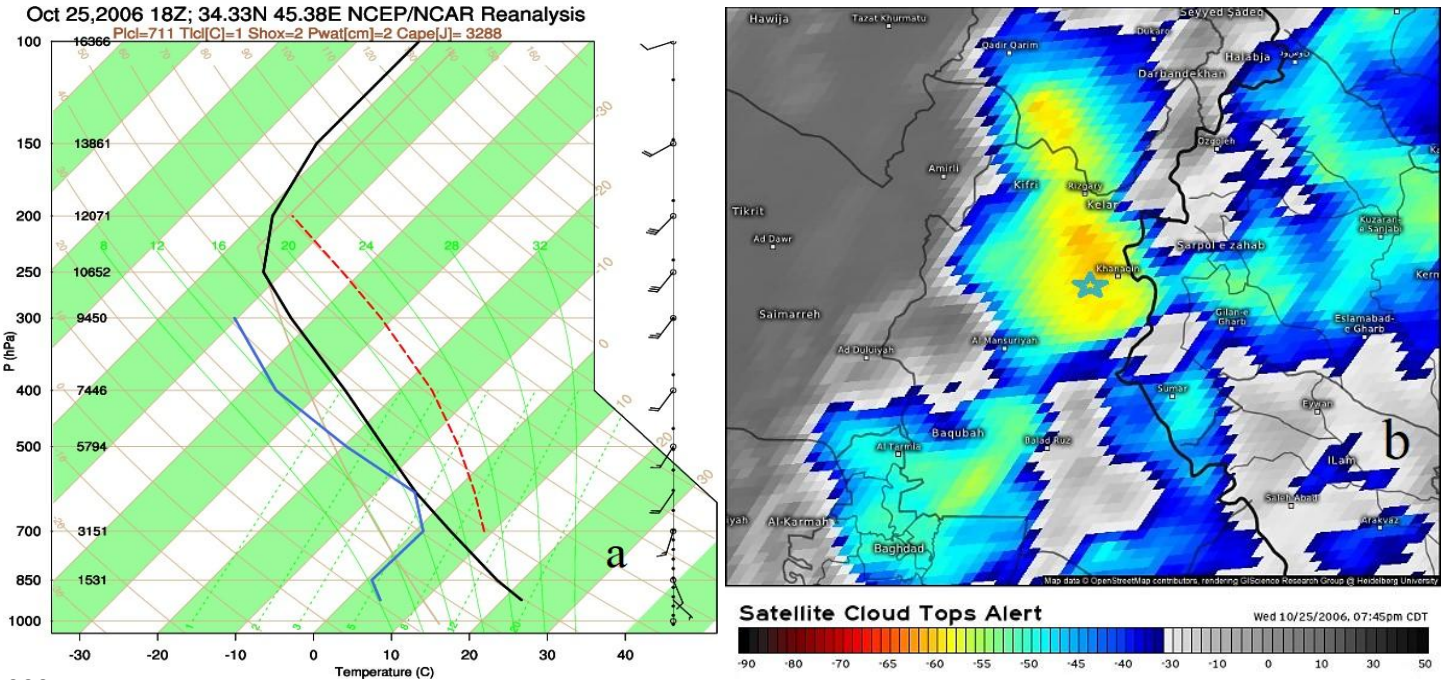


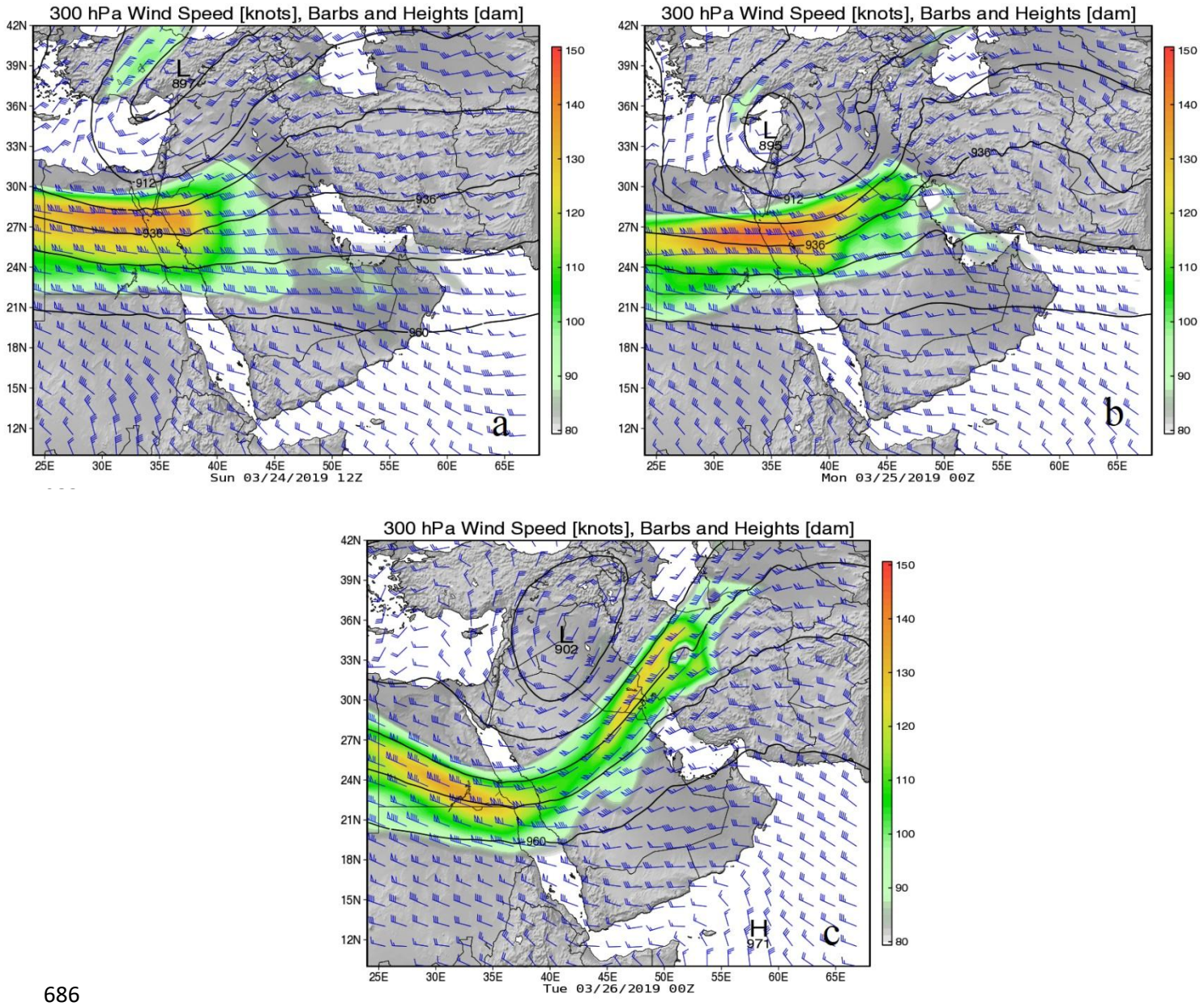
Figure 16. (a) Sounding data map on October 25, 2006; (b) Satellite imagery of cloud tops on October 25, 2006

5.1.2. Thunderstorm Case of March 24, 25, and 26, 2019 (Deep Mid-Latitude Depression)

On March 24, 2019, a thunderstorm was recorded at the Khanaqin station at 12:00. The maps in Figure 17 (A to C) show a time series of wind and geopotential height development at the 300 hPa level, which represents the core of the polar and subtropical jet streams. The polar jet stream is responsible for the dynamic control of instability in the Middle East. Panels (a-c) in Figures 17 and 18 show the development of the upper-level wave structure before, during, and after the formation of thunderstorms over Khanaqin. The maps show a dual jet stream system over the Middle East, represented by the presence of both the polar jet stream (PJ, in blue) over northern Iraq and the subtropical jet stream (STJ, in red) (Figure 18; A-C), extending from North Africa across the Arabian Peninsula toward Iran. This arrangement represents a dynamic pattern known in the literature as the Jet Coupling Pattern, where the spatial overlap between the acceleration and deceleration zones of the two jet streams leads to strong upper-level divergence zones (Keyser and Shapiro, 1986; Uccellini and Johnson, 1979).

In this case, Khanaqin City falls within the critical zone between the right entrance region of the polar jet stream and the left exit region of the subtropical jet stream. According to the subgeostrophic jet stream theory, these two zones are characterized by strong upper-level divergence resulting from an imbalance of Coriolis forces and pressure gradients, leading to a large-scale upward vertical movement (Bluestein, 1993; Holton and Hakim, 2013).

The direct result of this upper-level divergence is a decrease in air mass in the atmospheric column over eastern Iraq, which generates a hydrodynamic response of rising lower-level air to compensate for the mass deficit. With strong moisture flows via the southeasterly winds in the lower atmosphere, a high CAPE environment with strong dynamic forcing was created, providing ideal conditions for the formation of deep, organized thunderstorms (Doswell et al., 1996; Markowski and Richardson, 2010). In Figure 18 (A–C), the jet stream appears as a strong belt of winds exceeding 45–60 knots extending from North Africa across the eastern Mediterranean toward Iraq. The stream is characterized by a distinct deep Rossby wave trough centered west of Iraq and moving eastward.



686

687 **Figure 17.** Wind speed (knots) and direction and geopotential height (dam) at 300 hPa: (a) March 24, 2019; (b)
688 March 25, 2019; (c) March 26, 2019
689

690 - The blue path represents the polar jet stream, and the red path represents the subtropical jet stream in Figure 18
691 (a-b).

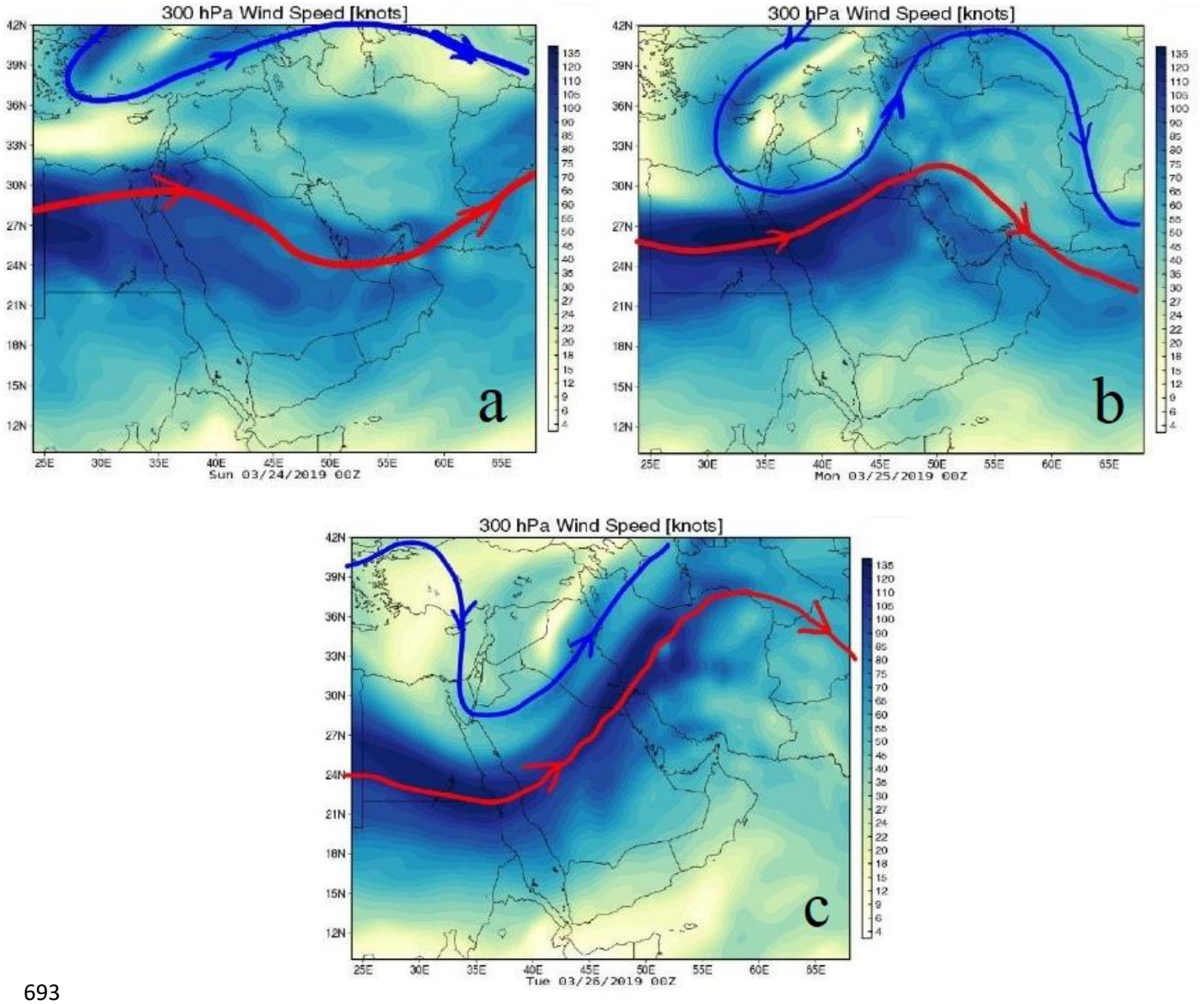


Figure 18. Wind speed (knots) and jet stream paths at 300 hPa: (a) March 24, 2019; (b) March 25, 2019; (c) March 26, 2019

The temperature and potential height maps at 500 hPa (Figure 19: A–C) show a classic temporal evolution of a deep cold-core upper-level trough over the eastern Mediterranean and Turkey, extending towards northern Iraq and western Iran. In phase A, a strong temperature gradient is observed over northern Iraq with very close potential height lines, indicating an active barocline zone separating the polar air mass to the north from the warm subtropical air to the south. In phase B, the trough deepens significantly and becomes a semi-cut-off upper-level trough, with temperatures dropping below −25°C at 500 hPa over northern Iraq, accompanied by a sharp drop in potential height values (570 dam). This structure implies a significant increase in vertical instability due to mid-troposphere cooling. In phase C, the trough moves eastward toward western Iran, but eastern Iraq (including Khanaqin) remains within the trough's forward-facing region, the most effective area for generating large-scale meso-level uplift.

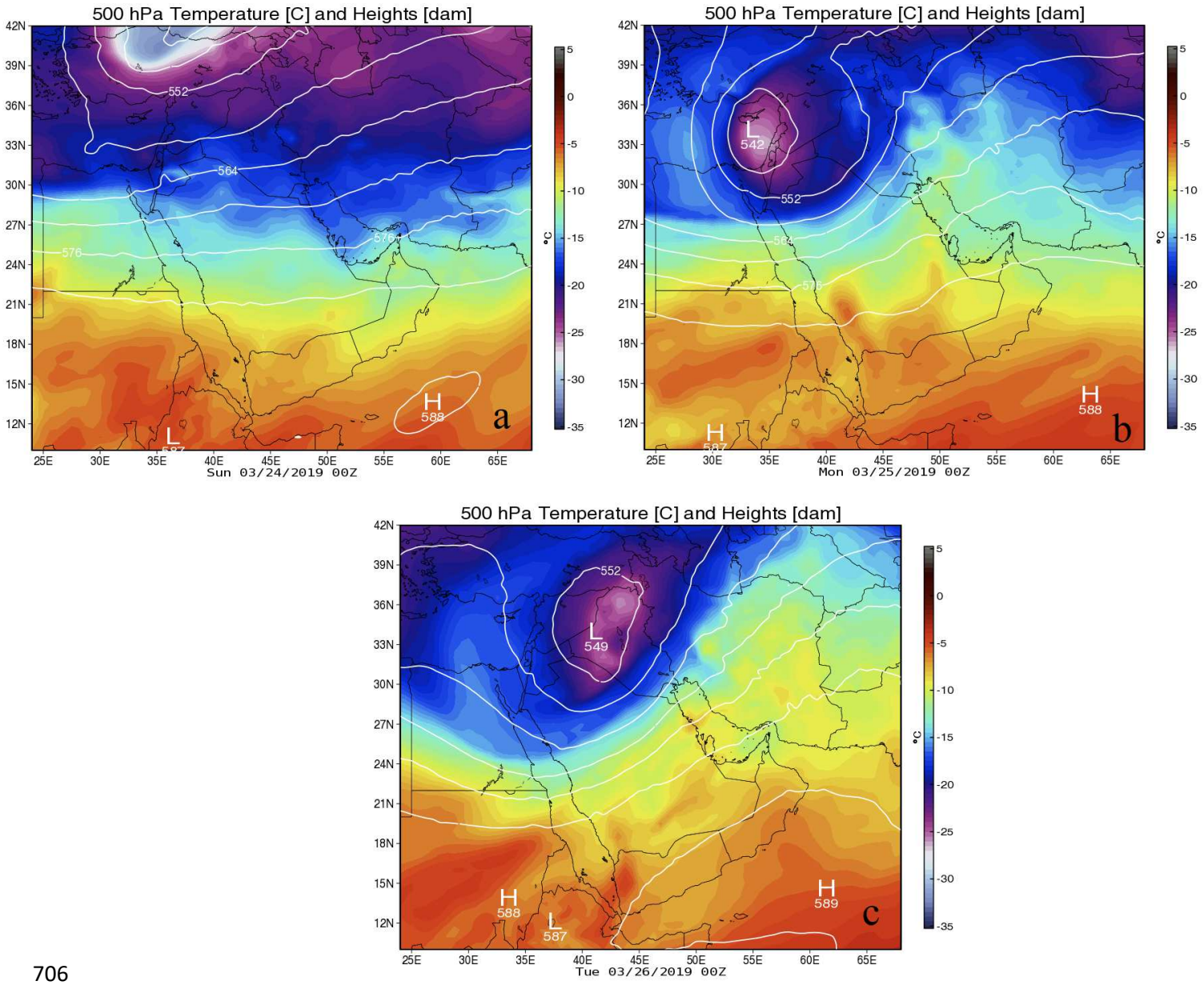


Figure 19. Air temperature (°C) and geopotential height (dam) at 500 hPa: (a) March 24, 2019; (b) March 25, 2019; (c) March 26, 2019

Surface temperature maps at 2 m (Fig. 20: A–C) show a direct response to the upper-level structure. In phase A, a sharp temperature contrast is observed between the following: A warm, moist air mass extending from the Arabian Gulf and Iran and a cooler air mass extending from northern Iraq and Turkey—a classic pattern for an active frontal region. In phase B, this temperature gradient intensifies as cold air pushes southward and warm air pushes northward, leading to the intensification of the frontal region over eastern Iraq. In phase C, Khanaqin remains within the air mass convergence zone, i.e., the frontogenesis zone, where the probability of both thermal uplift and dynamic uplift increases. The development of the 500 hPa cold trough and the surface front coincides with a coupling between the polar jet stream and the subtropical jet stream at 300 hPa. Khanaqin was located within the superposition region between the polar jet stream's right entrance and the subtropical jet stream's left exit, a region that generates the most upper-level divergence in the atmosphere (Holton and Hakim, 2013). Figures 19, 20, and 21 show that the Khanaqin situation was not the result of local surface heating, but rather the result of an interaction between three governing

systems: a cold upper-level trough at 500 hPa that increased the rate of vertical thermal depreciation; the coupling of the two jet streams at 300 hPa that generated strong upper-level divergence; and an active surface thermal front fueled by moisture from the Arabian Gulf. This interaction led to a drop in the atmospheric column pressure over eastern Iraq, forcing the warm, moist air in the lower layers to rise violently, transforming latent instability into deep, organized thunderstorms. This mechanism is similar to what is commonly observed in mid-latitude systems.

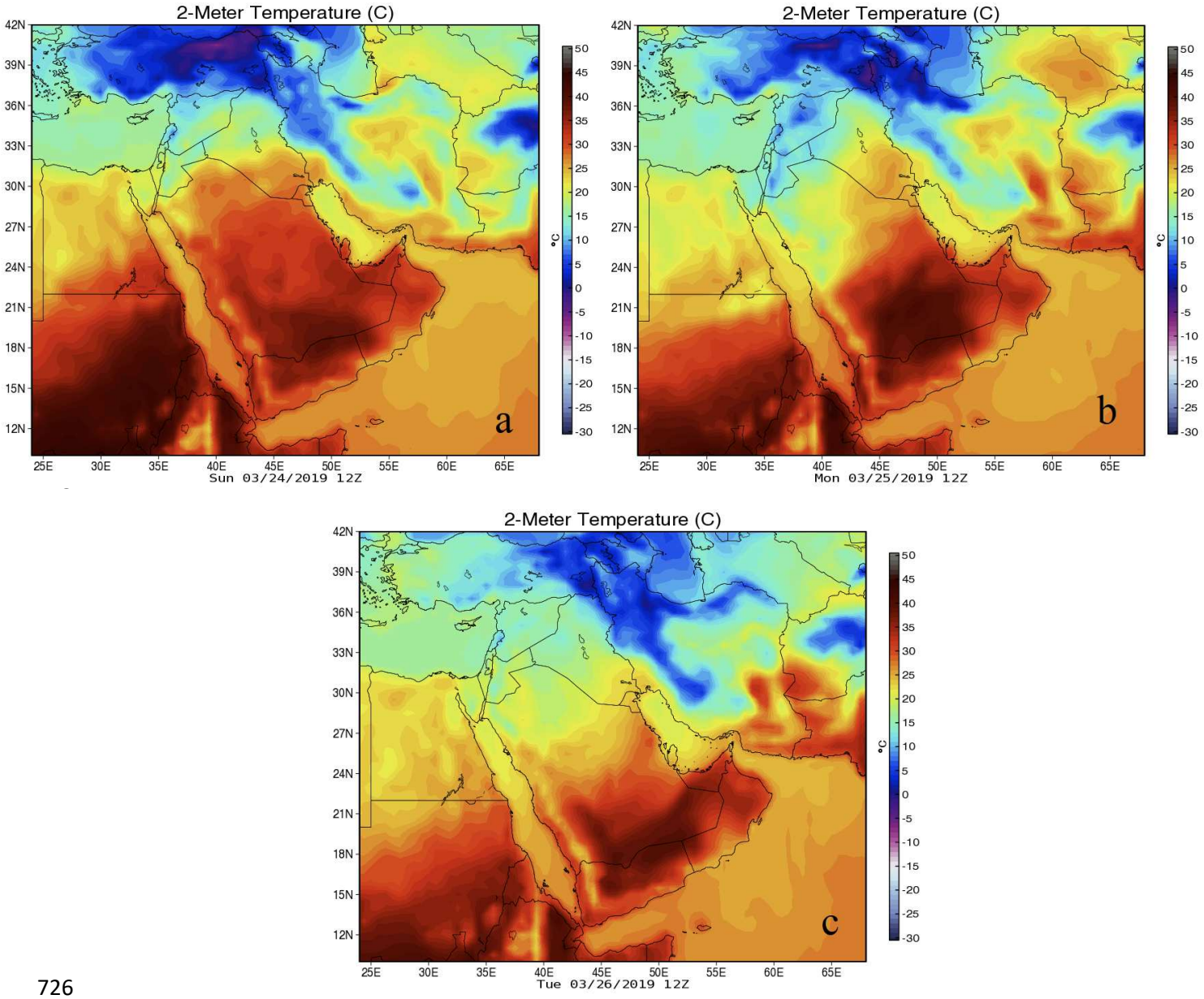


Figure 20. Air temperature distribution (°C) at a height of 2 meters: (a) March 24, 2019; (b) March 25, 2019; (c) March 26, 2019

The Skew-T/Log-P diagram shown in Figure (21a) illustrates the thermal and wind characteristics of the atmosphere over eastern Iraq during the peak of the event (March 24, 2019, 12Z). It clearly reveals that the atmosphere was in a state of deep conditional instability. This instability resulted from a clear divergence between the temperature and dew point curves in the middle layers, contrasted by a strong convergence in the lower layers. This indicates sufficient moisture in the surface layer; a relatively dry mid-level air intrusion; relatively high CAPE values (above

1200 J kg^{-1}), sufficient to support the development of strong updrafts capable of penetrating the middle and upper troposphere; and a weak or almost nonexistent CIN, meaning that synoptic lift mechanisms (jet + trough) were sufficient to generate convection without the need for intense surface heating. Strong vertical wind shear between 0–6 km, resulting from: This pattern is ideal for the development of multicell or supercell-like thunderstorm structures (Markowski and Richardson, 2010; Weisman and Klemp, 1982).

The presence of a dry air layer at mid-levels is a crucial element in amplifying storm intensity, leading to the following:

- Enhanced evaporative cooling
- Strengthened downdrafts
- Increased pressure differential within the thundercell.

This explains the violent nature of the storms recorded in Khanaqin, including the intensity and short duration of precipitation, a pattern common in semi-arid environments (Doswell, 2001).

The Satellite Cloud Tops Alert map in Figure 21b shows a wide range of frigid cloud tops (< −60°C) over eastern Iraq and western Iran, direct evidence of the development of deep convective towers and the arrival of updrafts at near-tropopause levels. The positioning of these tops coincides spatially and temporally with the jet stream overlap zone, the updraft zone ahead of the trough at 500 hPa, and the axis of the active surface front. This multi-scale consistency supports the conclusion that the thunderstorms in Khanaqin were caused by large-scale dynamic forcing rather than a localized disturbance.

- The blue line represents the dew point temperature, the black line represents the environment temperature, and the red line represents the CAPE value in Figure 21a.

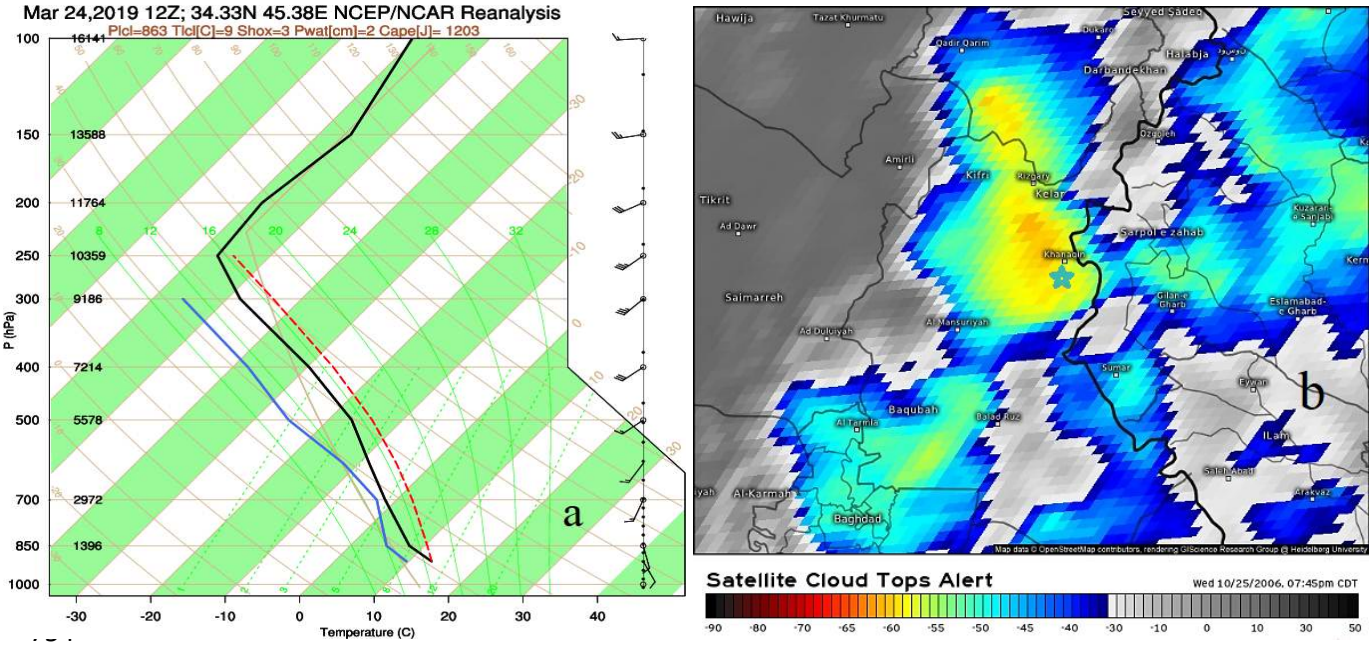


Figure 21. (a) Sounding data map on March 24, 2019; (b) Satellite imagery of cloud tops on March 24, 2019

6. Conflict of Interest Statement

The authors declare that they have no conflicts of interest to report.

7. Funding Statement

The researchers did not receive any specific grant from funding agencies in the public, commercial, or not-for-profit sectors.

8. Author Contributions

"All authors contributed to the study conception and design. Material preparation, data collection, and analysis were performed by [Imad Abdulridha Jasim Al-Khulaifawi] and [Aqeel Ghazi Mutar]. The first draft of the manuscript was written, and all authors commented on previous versions of the manuscript. All authors read and approved the final manuscript."

9. Data Availability

The datasets used in this study are publicly available and can be accessed as follows. ERA5 reanalysis data were obtained from the Copernicus Climate Change Service (C3S) through the European Centre for Medium-Range Weather Forecasts (ECMWF). [https://cds.climate.copernicus.eu/datasets/reanalysis-era5-pressure-levels?tab=download].

MERRA-2 reanalysis data were retrieved from the NASA Global Modeling and Assimilation Office (GMAO) data portal.
[https://fluid.nccs.nasa.gov/reanalysis/classic_merra2/?stream=MERRA2&field=wspd&level=300&fcst=20190324&region=mideast&tau=00&track=none].

Surface meteorological observations, including thunderstorm occurrence records, were provided by the Iraqi General Authority for Meteorology and Seismic Monitoring (GAMSM) and are available upon reasonable request from the corresponding authority and [https://meteologix.com/iq/reanalysis/ecmwf-era5/iraq].

10. Conclusions

This study provides a comprehensive analysis of thunderstorm activity over the city of Khanaqin in eastern Iraq for the period 1990–2019. This analysis integrates surface observational data, ERA5 reanalysis data, atmospheric instability indices, synoptic analysis, and studies of extreme weather events. The main conclusions can be summarized as follows:

1. The study results indicate that thunderstorm activity exhibits clear annual and seasonal variability, without a significant long-term trend toward either increase or decrease during the study period. This reflects the volatile climatic nature of the semi-arid environment in eastern Iraq.
2. Spring, particularly March and April, represents the peak of thunderstorm activity, accounting for over 40% of all events. This is attributed to the convergence of rising surface temperatures with increased humidity in the lower atmosphere and the frequent passage of mid-latitude low-pressure systems during the transitional seasons.
3. Atmospheric instability indicators revealed a predominantly moderately unstable atmospheric environment over the study area. K-index values ranged from 26 to 35, and Total Totals values from 45 to 52. CAPE values below 1000 J/kg constituted approximately 80% of the cases, indicating limited extreme conditions for thermal instability.
4. Despite the generally low CAPE values, the formation of deep, vertically extensive thunderstorms was frequently observed. This underscores the crucial role of large-scale dynamical influences, particularly upper-level troughs and wind variations in the upper atmosphere, in driving deep convection. Statistical analyses revealed clear physical relationships between thermal variables and cloud vertical structure. A significant positive linear correlation was found between surface temperature and both the low latitude condensation

level (LCL) and the equilibrium level (EL) (R = 0.7). The results also showed a strong non-linear relationship between CAPE and both EL and cloud thickness (R^2 = 0.6–0.7).

5. Atmospheric dynamics, particularly the coupling of the polar and subtropical jet streams, primarily influence thunderstorms in eastern Iraq, as indicated by synoptic analyses. This coupling enhances upper-level divergence and lower-level lifting, even under moderate thermal instability conditions.
6. The results indicated that shallow mid-latitude lows were more strongly associated with thunderstorms than deep lows. This reflects the transitional nature of the local climate and suggests a potential shift in storm patterns toward higher frequency and lower intensity under regional climate changes.
7. The frequent occurrence of deep convective clouds under moderate CAPE conditions highlights the dominant role of dynamic forcing. Upper-level wind shear and jet-induced divergence likely compensated for limited thermodynamic instability, emphasizing that CAPE alone is insufficient to characterize convective intensity in this region.

References

Agard, V., & Emanuel, K. (2017). Clausius–Clapeyron scaling of peak CAPE in continental convective storm environments. *Journal of the Atmospheric Sciences*, 74, 3043–3054. 10.1175/JAS-D-16-0352.1

Al-Ansari, N. (2013). Management of Water Resources in Iraq: Perspectives and Prognoses. *Engineering*, 05, 667-684. 10.4236/eng.2013.58080

Al-Ansari, N. (2021) Topography and Climate of Iraq. *Journal of Earth Sciences and Geotechnical Engineering*, 11, 1-13. DOI: 10.47260/jesge/1121

AL Lami, A. M., Al Timimi, Y. K., & Al Salihi, A. M. (2024). Innovative trend analysis of annual rainfall in Iraq during 1980-2021. *Journal of Agrometeorology*. 10.54386/jam.v26i2.2561

Al-Khulaifawi, Imad & Ruvimovich, Ioshpa. (2025). A Decade of Thunderstorm Patterns: A Comparative Study of Iraq and Russia. *Iraqi Journal of Science*. 3018-3027. DOI: 10.24996/ijs.2025.66.7.28

Al-Khulaifawi, Imad & Mutar, Aqeel. (2026). Thundercloud assessment for the years 1990–2019 over the Baghdad airport station. https://doi.org/10.21203/rs.3.rs-8683928/v1

Al Muhyi, H., Aleedani, F. Y., Albattat, M. Q., & Badr, J. M. (2024). Rainfall Repercussions: Assessing Climate Change Influence on Iraq Precipitation Patterns. *Al Kitab Journal for Pure Sciences*. 8, 92-103. 10.32441/kjps.08.01.p9

Bluestein, H. B. (1993). *Synoptic-Dynamic Meteorology in Midlatitudes: Volume II: Observations and Theory of Weather Systems*. Oxford University Press, New York, 594 p.

Brázdil, R., Chromá, K., Púčik, T., et al. (2020). The climatology of significant tornadoes in the Czech Republic. *Atmosphere*, 11(7). 10.3390/atmos11070689

Buck, A. L. (1981). New equations for computing vapor pressure and enhancement factor. *Journal of Applied Meteorology*, 20, 1527-1532. 10.1175/1520-0450(1981)020<1527:NEFCVP>2.0.CO;2

Cinaroglu, Eda & Unutulmaz, Osman. (2018). A Data Mining Application of Local Weather Forecast for Kayseri Erkilet Airport. *Journal of Polytechnic*. 10.2339/politeknik.391801

Craven, J. P., Jewell, R. E., & Brooks, H. E. (2002). Comparison between observed convective cloud-base heights and lifting condensation level for two different lifted parcels. *Weather and Forecasting*, *17*(4), 885–890. 10.1175/1520-0434(2002)017<0885:CBOCCB>2.0.CO;2

Dai, A. (2006). Recent climatology, variability, and trends in global surface humidity. *Journal of Climate*, 19, 3589–3606. 10.1175/JCLI3816.1

Doswell, C. A. III. (1987). The distinction between large-scale and mesoscale contribution to severe convection: a case study example. *Weather and Forecasting*, 2(1), 3–16. 10.1175/1520-0434(1987)002<0003:TDBLSA>2.0.CO;2

Doswell, C.A., Brooks, H.E., and Maddox, R.A. (1996). Flash Flood Forecasting: An Ingredients-Based Methodology. Weather and Forecasting, 11, 560-581. https://doi.org/10.1175/1520-0434(1996)011<0560:FFFAIB>2.0.CO;2

Doswell, C. A. (2001). Severe convective storms—An overview. *Meteorological Monographs*, 28(50), 1–26. 10.1175/0065-9401-28.50.1

Emanuel, K. A. (1994). *Atmospheric convection*. New York, NY: Oxford University Press.

George, J. J. (1960). *Weather and Forecasting for Aeronautics*. Academic Press, Waltham, MA.

Gettleman, A., Seidel, D., Wheeler, M., & Ross, R. (2002). Multi-decadal trends in tropical convective available potential energy. *Journal of Geophysical Research*, 107(D21), 4606–4614. 10.1029/2001JD001082

Gray, W. M., & Jacobson Jr., R. W. (1977). Diurnal Variation of Deep Cumulus Convection. *Monthly Weather Review*, 105(9), 1171-1188. https://doi.org/10.1175/1520-0493(1977)105<1171:DVODCC>2.0.CO;2

Hersbach, H., Bell, B., Berrisford, P., et al. (2023). ERA5 hourly data on pressure levels from 1940 to present. *Copernicus Climate Change Service (C3S) Climate Data Store (CDS)*. DOI: 10.24381/cds.bd0915c6

Holton, J. R., & Hakim, G. J. (2013). *An introduction to dynamic meteorology*. 5th Edition, Academic Press, Cambridge, 552 p. https://doi.org/10.1016/C2009-0-63394-8

Humood, B. Y., & Abbas, L. M. (2017). Studying recorded lightning over Iraq for period 1998-2011. *Al-Mustansiriyah Journal of Science*, 28, 1-6. http://doi.org/10.23851/mjs.v28i3.50

Hussain A., N, Thaer O., R, & Zahraa F. R. (2025). Synoptic Analysis of Polar and Subtropical Jet Streams and their Influences on Baghdad City. *An-Najah University Journal for Research – A Natural Sciences*, 40(3), 1-11. 10.35552/anujr.a.40.2.2613

Ibrahim, I. A., & Al-Dabbas, M. (2021). Analysis of Climate Parameters as Indicators of Climate Changes in Central and Eastern Iraq: Khanaqin Climate Conditions as A Case Study. *Iraqi Journal of Science*, 62(12), 4747–4757. https://doi.org/10.24996/ijs.2021.62.12.13

Ioshpa, A. R., & Al-Khulaifawi, I. A. J. (2023). Analysis of thunderous activity in Iraq. *News of Higher Educational Institutions. North Caucasus Region. Natural Sciences*, 218 (2), 75–80. doi: 10.18522/1026-2237-2023-2-75-80

Keyser, D., & Shapiro, M. A. (1986). A review of the structure and dynamics of upper-level frontal zones. *Monthly Weather Review*, 114(2), 452–499. https://doi.org/10.1175/1520-0493(1986)114〈0452:AROTSA〉2.0.CO;2

Khidher, S., & Pilesjö, P. (2014). The effect of the North Atlantic Oscillation on the Iraqi climate 1982–2000. *Theoretical and Applied Climatology*, 122. doi. 10.1007/s00704-014-1327-4

Kolay, O., Efe, B., Özdemir, E. T., & Aslan, Z. (2025). A multi-year investigation of thunderstorm activity at Istanbul International Airport using atmospheric stability indices. *Atmosphere*, 16(4), 470. 10.3390/atmos16040470

Kolendowicz, L., Taszarek, M., & Czernecki, B. (2017). Atmospheric circulation and sounding-derived parameters associated with thunderstorm occurrence in Central Europe. *Atmospheric Research*, 191, 101–114. https://doi.org/10.1016/j.atmosres.2017.03.009

Krider, E. P. (2021). "Thunderstorm." *Encyclopedia Britannica*. Retrieved 14 January 2021. https://www.britannica.com/science/thunderstorm

Laura López, José Luis Marcos, José Luis Sánchez, Amaya Castro, and Roberto Fraile. (2001). CAPE values and hailstorms on northwestern Spain. *Atmospheric Research*, 56(1), 147-160. DOI: 10.1016/S0169-8095(00)00095-8

Leena, P. P., Pandithurai, G., Gayatri, K., et al. (2019). Analysing the characteristic features of a pre-monsoon thunderstorm event over Pune, India, using ground-based observations and WRF model. *Journal of Earth System Science*, 128, 108. https://doi.org/10.1007/S12040-019-1136-3

Lucas, C., Zipser, E. J., & LeMone, M. A. (1994). Convective available potential energy in the environment of oceanic and continental clouds: correction and comments. *J. Atmos. Sci.*, 51(24), 3829–3830. https://doi.org/10.1175/1520-0469(1994)051<3829:capeit>2.0.co;2

Madhulatha, A., Rajeevan, M., Venkat Ratnam, M., et al. (2013). Nowcasting severe convective activity over southeast India using ground-based microwave radiometer observations. *Journal of Geophysical Research: Atmospheres*, 118, 1–13. https://doi.org/10.1029/2012JD018174

Markowski, P., & Richardson, Y. (2010). *Mesoscale meteorology in midlatitudes*. Wiley-Blackwell. 10.1002/9780470682104

Mathew, T. A., Malap, N., Manoj, M. G., et al. (2021). Pre-monsoon convective events and thermodynamic features of southwest monsoon onset over Kerala, India—a case study. *Atmospheric Research*, 248, 105218. 10.1016/j.atmosres.2020.105218

Miller, R. C. (1972). Notes on Analysis and Severe Storm Forecasting Procedures of the Air Force Global Weather Central. *Tech. Rept*. 200(R), Headquarters, Air Weather Service, USAF, 190p.

Mutar, A., Abdulkareem, A., & George, L. (2021). Synoptic Characteristics of Torrential Rains in Southwest and Southeast Iraq: A Case Study. *Al-Mustansiriyah Journal of Science*, 32(3). 10.23851/mjs.v32i3.957

NSSL. (2020). *SEVERE WEATHER 101 / Thunderstorm Basics*. National Severe Storms Laboratory, NOAA. https://www.nssl.noaa.gov/education/svrwx101/thunderstorms/

NWS (National Weather Service). (2022). Definition of atmospheric variables, atmospheric stability indices. https://www.weather.gov/ffc/gloss2

Pekárová, P., Mészáros, J., Miklánek, P., et al. (2021). Post-flood field investigation of the June 2020 flash flood in the upper Muráň River basin and the catastrophic flash flood scenario. *Journal of Hydrology and Hydromechanics*. https://doi.org/10.2478/johh-2021-0015

Púčik, T., Valachová, M., & Zacharov, P. (2013). Upper tropospheric conditions in relation to the cloud top features of 15 August 2010 convective storms. *Atmospheric Research*, 123, 249–267. https://doi.org/10.1016/j.atmosres.2012.10.006

Peterson, M., Rudlosky, S., & Zhang, D. (2020). Thunderstorm cloud-type classification from space-based lightning imagers. *Monthly Weather Review*, 148(5), 1891–1898. https://doi.org/10.1175/mwr-d-19-0365.1

Ratnam, M. V., Santhi, Y. D., Rajeevan, M., & Rao, S. V. B. (2013). Diurnal variability of stability indices observed using radiosonde observations over a tropical station. *Atmospheric Research*, 124, 21-33. http://dx.doi.org/10.1016/j.atmosres.2012.12.007

Romps, D. M. (2016). Clausius–Clapeyron scaling of CAPE from analytical solutions to RCE. *Journal of the Atmospheric Sciences*, 73, 3719–3737. 10.1175/JAS-D-15-0327.1

Roy, P., Rao, T. N., Biswasharma, R., et al. (2023). Space–time variation of large hail-producing mesoscale convective systems over a complex terrain of the Indian subcontinent. *International Journal of Climatology*, 43(6), 3023–3039. https://doi.org/10.1002/joc.8015

Shmeter, S. M. (1972). *Fizika konvektivnykh oblakov* [Physics of Convective Clouds]. Leningrad: Gidrometeoizdat.

Showalter, A. K. (1953). A stability index for forecasting thunderstorms. *Bull. Amer. Meteor. Soc.,* 34, 250-252. 10.1175/1520-0477-34.6.250

Sinkevich, A. A., Mikhailovskii, Y. P., Dovgalyuk, Y. A., et al. (2016). Investigations of the development of thunderstorm with hail (Part 1). *Russian Meteorology and Hydrology*, 41, 610-619. 10.3103/S106837391609003X

Sokol, Z., Popová, J., Skripniková, K., et al. (2023). Comparison of cloud structures of storms producing lightning at different distance based on five years measurements of a Doppler polarimetric vertical cloud profiler. *Remote Sensing*, 15(11), 2874. 10.3390/rs15112874

Sultan, A. G. (1986). *Climate, its elements and changes*. Baghdad: Baghdad Publishing House. 480p. (in Arabic).

Tao, W. K., et al. (2022). Relating vertical velocity and cloud/precipitation properties. *Journal of Advances in Modeling Earth Systems*. https://doi.org/10.1029/2021MS002677

Taszarek, M., Allen, J. T., Groenemeijer, P., et al. (2020). Severe convective storms across Europe and the United States. *Journal of Climate*, 33, 10239–10261. https://doi.org/10.1175/JCLI-D-20-0345.1

Taylor, K. E., Stouffer, R. J., & Meehl, G. A. (2012). An overview of CMIP5 and the experiment design. *Bulletin of the American Meteorological Society*, 93(4), 485–498. 10.1175/BAMS-D-11-00094.1

U.S. Department of Defense. (1990). *The use of the skew T, log P diagram in analysis and forecasting*. Technical report. https://unidata.github.io/MetPy/latest/_static/USAF_SkewT_manual.pdf

Uccellini, L. W., & Johnson, D. R. (1979). The coupling of upper and lower tropospheric jet streaks and implications for the development of severe convective storms. *Monthly Weather Review*, 107(5), 682–703. https://doi.org/10.1175/1520-0493(1979)107

Umakanth, N., Biswasharma, R., Gogineni, R. et al. (2024). Relationship between TTI and Various Thunderstorm Related Parameters over Kerala, India. *Pure Appl. Geophys.* 181(11), 3331–3350. DOI: 10.1007/s00024-024-03617-7

Wang, P. K. (2013). "Observation of clouds", in *Physics and Dynamics of Clouds and Precipitation*. https://doi.org/10.1017/CBO9780511794285

Weisman, M. L., & Klemp, J. B. (1982). The dependence of numerically simulated convective storms on vertical wind shear and buoyancy. *Monthly Weather Review*, 110, 504–520. https://doi.org/10.1175/1520-0493(1982)110

Willett, K. M., Phillip, P. D., Thorne, P. W., & Gillett, N. P. (2010). A comparison of large-scale changes in surface humidity over land in observations and CMIP3 models. *Environmental Research Letters*, 5(2):025210. 10.1088/1748-9326/5/2/025210

World Meteorological Organization. (2024). Guide to instruments and methods of observation (WMO-No. 8). https://wmo.int/guide-instruments-and-methods-of-observation-wmo-no-8-0

World Meteorological Organization. (2024). State of the climate in the Arab region 2024. https://wmo.int/files/state-of-climate-arab-region-2024

Xu, D., You, X., & Xia, C. (2019). Assessing the spatial-temporal pattern and evolution of areas sensitive to land desertification in North China. *Ecological Indicators*, 97, 150-158. https://doi.org/10.1016/j.ecolind.2018.10.005

Ye, B., Genio, A.D.D., & Lo, K.K.W. (1998). CAPE variations in the current climate and in a climate change. *J. Clim.*, 11(8), 1997–2015. https://doi.org/10.1175/1520-0442

Zhao, C., Zhang, Y., Zhai, H., et al. (2025). Bridging the polarimetric structure and lightning activity of isolated thunderstorm cells during the cloud life cycle. *Atmospheric Chemistry and Physics*, 25(20), 13453–13473. 10.5194/acp-25-13453-2025